Invited, Rapporteur, and Highlight papers of ICRC 2001: 21

ICRC 2001

From solar min to solar max: half a solar cycle of SOHO observations

P. Brekke and B. Fleck

ESA Space Science Department, NASA/GSFC
Mailcode 682.3 Greenbelt, MD 20771, USA

Abstract. The Solar and Heliospheric Observatory (SOHO) has provided an unparalleled breadth and depth of information about the Sun, from its interior, through the hot and dynamic atmosphere, out to the solar wind. Analysis of the helioseismology data from SOHO has shed new light on a number of structural and dynamic phenomena in the solar interior, such as the absence of differential rotation in the radiative zone, subsurface zonal and meridional flows, subconvection-zone mixing, a possible circumpolar jet, and very slow polar rotation. Evidence for an upward transfer of magnetic energy from the Sun's surface toward the corona has been established. The ultraviolet instruments have revealed an extremely dynamic solar atmosphere where plasma flows play an important role. Electrons in coronal holes were found to be relatively 'cool', whereas heavy ions are extremely hot and have highly anisotropic velocity distributions. The source regions for the high speed solar wind has been identified and the acceleration profiles of both the slow and fast solar wind have been measured. This paper tries to summarize some of the findings from the SOHO mission from the past five years.

1 Introduction

SOHO, the Solar and Heliospheric Observatory, is a project of international cooperation between ESA and NASA to study the Sun, from its deep core to the outer corona, and the solar wind (Domingo et al., 1995). It carries a complement of twelve sophisticated instruments, developed and furnished by twelve international PI consortia involving 39 institutes from fifteen countries (Belgium, Denmark, Finland, France, Germany, Ireland, Italy, Japan, Netherlands, Norway, Russia, Spain, Switzerland, United Kingdom, and the United States). Detailed descriptions of all the twelve instruments on board SOHO as well as a description of the SOHO ground system, science operations and data products together with a mission overview can be found in Fleck et al. (1995).

SOHO has a unique mode of operations, with a 'live' display of data on the scientists' workstations at the SOHO Experimenters' Operations Facility (EOF) at NASA Goddard Space Flight Center, where the scientists can command their instruments in real-time, directly from their workstations. From the very beginning SOHO was conceived as an integrated package of complimentary instruments. It was once described pointedly as an "object-oriented mission, rather than an instrument oriented mission". Great emphasis is therefore being placed on coordinated observations. Internally, this is facilitated through a nested scheme of planning meetings (monthly, weekly, daily), and externally through close coordination and data exchange for special campaigns and collaborations with other space missions and ground-based observatories over the Internet

Once cannot adequately cover over 1000 articles in the refereed literature and over 1500 articles that appeared in conference proceedings and other publications. Instead, we can only touch upon some selected results.

2 Global structure and dynamics of the solar interior

Just as seismology reveals the Earth's interior by studying earthquake waves, solar physicists probe inside the Sun using a technique called 'helioseismology'. The oscillations detectable at the visible surface are due to sound waves reverberating through the Sun's interior. These oscillations are usually described in terms of normal modes that are identified by three integers: angular degree l, angular order m, and radial order n. The frequencies of the normal modes depend on the structure and flows in the regions where the modes propagate. Because different modes sample different regions inside the Sun, by observing many modes one can, in principle, map the solar interior. By measuring precisely the mode frequencies, one can infer the temperature, density, equation of state, elemental and isotopic abundances, interior mixing,

Correspondence to: P. Brekke
(pbrekke@esa.nascom.nasa.gov)

interior rotation and flows, even the age of the solar system, and pursue such esoteric matters as testing the constancy of the gravitational constant ($(1/G)dG/dt$), which from a recent study by Guenther et al. (1998) must be smaller than $1.6 \times 10^{-12}\mathrm{yr}^{-1}$.

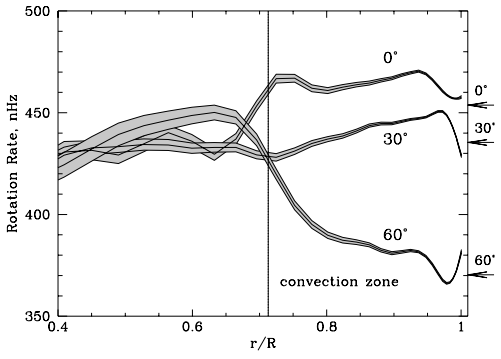

Fig. 1. Inferred rotation rate as a function of depth and latitude. Evidently the convection zone rotates uniformly along a radius with all depths showing the differential rotation seen at the surface. Below the convection zone is a layer of shear below which the radiative interior seems to rotate rigidly. This shear zone which coincides with the sound speed excess could be the region where the solar cycle dynamo operates (From Kosovichev, Schou, and Scherrer, 1997).

2.1 Interior rotation and flows

The nearly uninterrupted data from the Michelson Doppler Imager (MDI) yield oscillation power spectra with an unprecedented signal-to-noise ratio that allow the determination of the frequency splittings of the global resonant acoustic modes of the Sun with exceptional accuracy. The inversions of these data have confirmed that the decrease of the angular velocity Ω with latitude seen at the surface extends with little radial variation through much of the convection zone, at the base of which is an adjustment layer, called the "tachocline", leading to nearly uniform rotation deeper in the radiative interior (Kosovichev et al. 1997; Schou et al. 1998) (Fig. 1). Further a prominent rotational shearing layer in which Ω increases just below the surface is discernible at low to mid latitudes. The MDI team has also been able to study the solar rotation closer to the poles than has been achieved in previous investigations. The data have revealed that the angular velocity is distinctly lower at high latitudes than the values previously extrapolated from measurements at lower latitudes based on surface Doppler observations and helioseismology (Birch and Kosovichev 1998).

From f-mode frequency splittings of MDI data, Kosovichev and Schou (1997) detected zonal variations of the Sun's differential rotation, superposed on the relatively smooth latitudinal variation in Ω. These alternating zonal bands of slightly faster and slower rotation show velocity variations of about 5 m s^{-1} at a depth of 2-9 Mm beneath the surface and extend some 10 to 15 deg in latitude. They appear to coincide with the evolving pattern of 'torsional oscillations' reported from earlier surface Doppler studies. Schou et al. (1998) followed these relatively weak banded flows down to a depth of about 5% of the solar radius. In a later study of the time evolution of these flows, Schou (1999) found clear evidence of the migration of these zonal flows toward the equator. The contrast of the bands seems to be increasing with time.

Antia and Basu (2001) studied temporal variations of the solar rotation rate using GONG and MDI data from May 1995 through April 2001. The rotation rate residuals show the well- known pattern of temporal variations similar to the torsional oscillations observed at the surface, with bands of faster and slower rotation moving toward the equator with time at low to mid latitudes. Above 50 deg latitude, the bands move to the pole instead, similar to the poleward movement of magnetic features observed at high latitudes. It is interesting to note that some mean field dynamo models also show this feature (e.g. Covas et al., 2000). These results therefore reinforce the link between zonal flows and the solar magnetic cycle. The rotation rate in the outer layers of the polar regions varies with time, reaching a minimum in early 1999 (i.e. distinctly before the maximum of solar activity!), after which it has started increasing again. Similarly, it appears that the maximum rotation rate was achieved before the minimum in activity. These changes appear to persist down to a depth of about $0.1\mathrm{R}_\odot$, similar to the depth of penetration of the zonal flow pattern at low latitudes.

Howe et al. (2000b) also used global p-modes to detect the zonal flows of the torsional oscillation, and found that these penetrate to a depth of at least 56 Mm (Fig. 2). This work led to the detection of a variation in the rotation rate near the bottom of the convection zone with a 1.3 year period as shown in Fig. 3 (Howe et al. 2000a). This variation and its implications are not yet understood. It has withstood a number of tests of reality and the result remains intact. We anticipate the opportunity of seeing what happens in the declining phase of the solar cycle.

Beck et al. (1998) have detected long-lived velocity cells in autocorrelation functions calculated from a 505 day time series of MDI data. These cells extend over 40-50 degrees of longitude but less than 10 degrees of latitude. The authors identify these cells with the elusive 'giant cells', although their large aspect ratio ($\geq$4) is surprising. It may be a consequence of the Sun's differential rotation, whereby features with a larger extent in latitude are broken up by rotational shear.

High precision MDI measurements of the Sun's shape and brightness obtained during two special 360 deg roll manoeuvres of the SOHO spacecraft have produced the most precise determination of solar oblateness ever (Kuhn et al. 1998). There is no excess oblateness. These measurements unambiguously rule out the possibility of a rapidly rotating core, and any significant solar cycle variation in the oblateness.

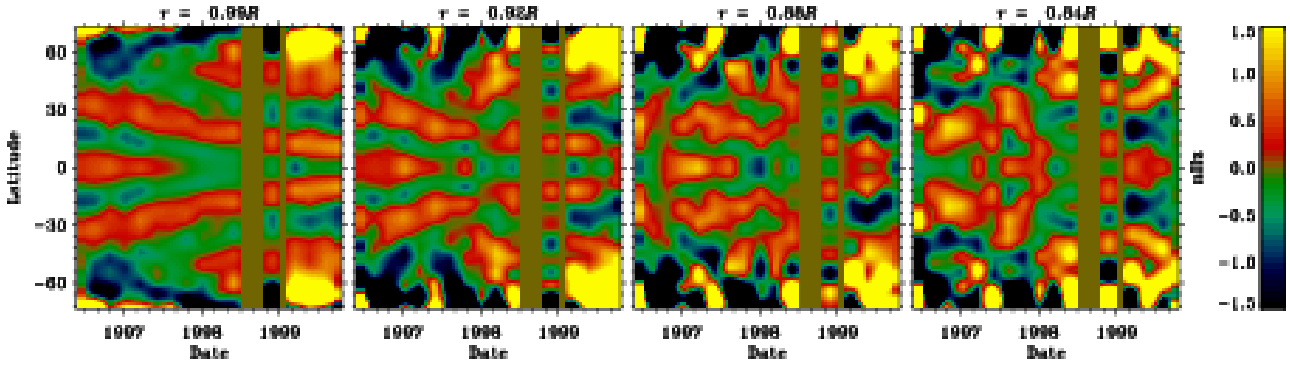

Fig. 2. Migrating banded zonal flows. Variation of rotation rate with latitude at four different depths in the convection zone. The uniform vertical bands indicate time periods when no data were available from SOHO (during the summer of 1998 due to the temorary loss of spacecraft, and in January 1999 when SOHO was in safe mode after a gyroscope failure). The scale to the right indicates the dynamic range in nHz of the angular velocity. (From Howe et al. 2000b)

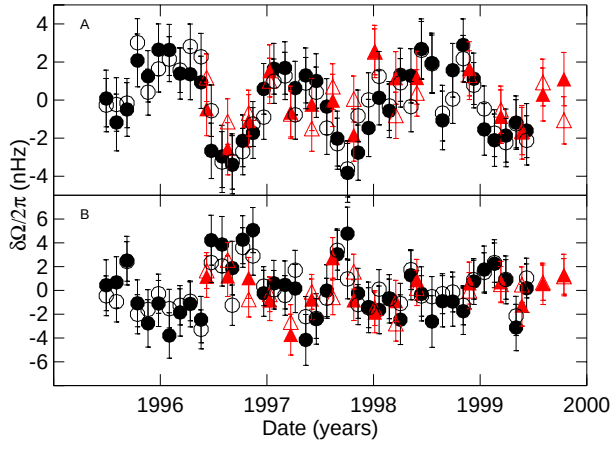

Fig. 3. Time variation of rotation rates at 0.72 (upper) and 0.63 (lower) solar radii, on each side of the tachocline. Results from GONG data using two different methods are shown in black, results from MDI are shown in grey (Howe et al. 2000a).

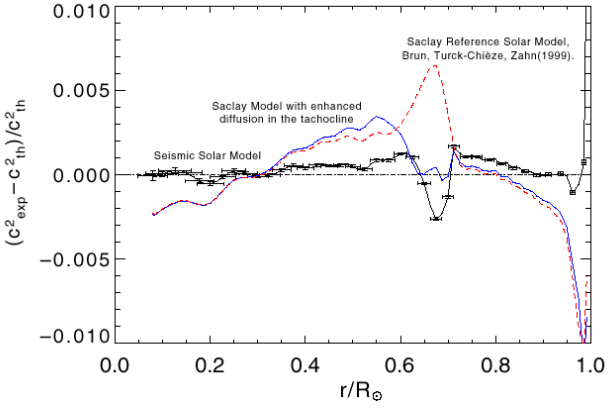

Fig. 4. A recent model of the solar interior is able to resolve sound speed discrepancies with earlier models. The plot shows the relative differences between the squared sound speed in the Sun as observed by GOLF and MDI and a reference model (dashed line). (From Turck-Chiéze et al. 2001.)

2.2 Interior sound speed profile

The availability of helioseismic data of unprecedented accuracy from the SOHO MDI, GOLF, and VIRGO instruments has enabled substantial improvements in models of the solar interior, and have even shown the importance of considering mixing effects that turn out to solve existing riddles in the isotopic composition of the Sun.

Fig. 4 shows the relative difference between the squared sound speed in the Sun as observed by GOLF and MDI and a reference model (solid line) and two models including macroscopic mixing processes in the tachocline (dashed and dash-dotted lines). Similar diagrams (as the solid line) have been produced by various other groups. This figure is quite remarkable: There is a very good agreement between the measured sound speed and the model throughout most of the interior. Except at the conspicuous bump at about 0.68 $R_\odot$ (the location of the transition from the radiative zone into the convection zone) the difference is less than 0.2%, suggesting that our understanding of the mean radial stratification of the Sun is not too far off.

In order to resolve this discrepancy at 0.68 $R_\odot$ and the failure of recent updated standard models to predict the photospheric lithium abundance, Brun et al. (1999) introduced a new term — macroscopic mixing below the convective zone — in the standard stellar structure equations. They showed that the introduction of mixing in the tachocline layer partly inhibits the microscopic diffusion process and significantly improves the agreement with the helioseismic data and photospheric abundance data. In particular, the prominent bump around 0.68 $R_\odot$ in the sound-speed square difference plot is practiacally erased by the introduction of the tachocline mixing (see the dash-dotted line in Fig. 4). With this new term it is also possible to reach the observed ^{7}Li photospheric abundance at the present solar age without destroying ^{9}Be

or bringing too much ^{3}He to the surface. The solar ^{4}He primordial abundance would be slightly enriched by 10.6% to Y_0=0.27. As the process invoked concerns only the 5% part of the external mass it has little impact on the neutrino flux (only a slight reduction of a few percent).

Bertello et al. (2000) and Garcia et al, (2001) have recently identified and measured the frequencies of several new, low frequency modes in GOLF data, using the asymmetric fitting methods pioneered by Toutain et al. (1998) to match MDI and VIRGO LOI measurements. These mode frequencies have been combined with results from higher l modes and higher frequency modes (measured by MDI) to yield a new "Seismic Solar Model". In this model, the abundances and the cross- section for the proton-proton reaction have been modified within their acceptable error range to adjust the model toward best agreement between the deduced frequencies and those observed from MDI and GOLF. Because the solar model is now constrained by the helioseismic data, the errors mostly reflect the comparison of two different sets of measurements (helioseismic frequencies and neutrino counting rates) instead of errors in the input physics. This result indicates that the discrepancy must be resolved by means of modified neutrino physics.

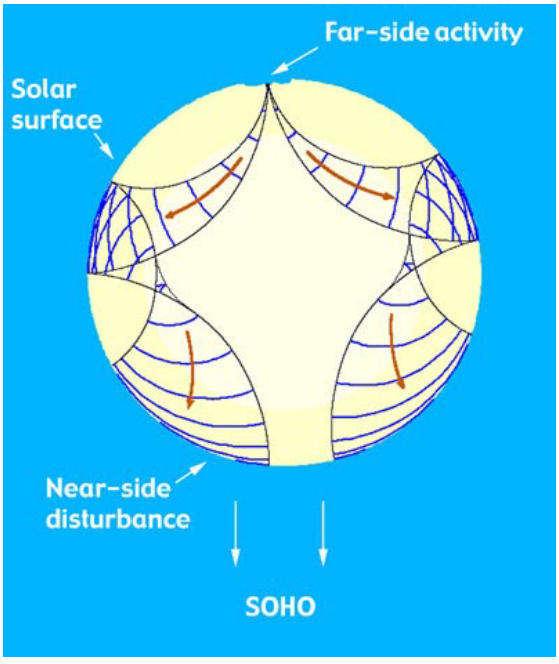

Fig. 5. Sound waves from the far side of the Sun are reflected internally once before reaching the front side, where they are observed with MDI. (Courtesy MDI consortium)

3 Local area helioseismology

In conventional helioseismology, most results are obtained from a global mode analysis. A time series of velocity or intensity images is decomposed into eigenmodes, characterized by radial order n, spherical harmonic degree l, and azimuthal order m. The eigenfrequencies of the eigenmodes provide the global information on the spherically symmetric and axisymmetric components of the solar interior. Recently, with the availability of high spatial resolution data from MDI, interest in studying the local structure of the Sun in helioseismology has grown rapidly. There are several new techniques being developed. We mention three of them: helioseismic holography (and acoustic imaging), ring diagrams, and time-distance helioseismology.

3.1 Helioseismic holography

A technique called "helioseismic holography", originally proposed by Roddier in 1975 (although not using the term "holography"), has been applied to MDI data to render acoustic images of the absorption and egression of sunspots and active regions (Braun et al., 1998; Lindsey and Braun, 1998a, 1998b). The images revealed a remarkable acoustic anomaly surrounding sunspots, now called the "acoustic moat" (Lindsey and Braun, 1998a), which is a conspicuous halo of enhanced acoustic absorption at 3 mHz. At 5–6 mHz, on the other hand, a prominent halo of enhanced acoustic emission (now called "acoustic glory") was found surrounding active regions (Braun and Lindsey, 1999). Lindsey and Braun (1999) obtained "chromatic" images over the 3–8 mHz acoustic spectrum, showing the acoustic moat out to 4.5 mHz and its disappearance at higher frequencies. Helioseismic holography essentially applies the helioseismic observations in an extended annulus surrounding the proposed source to an acoustic model of the solar interior in time reverse, regressing the acoustic field into the model interior to render images of supposed acoustic sources that can be sampled at any desired depth. This technique was recently applied to MDI data to derive the first seismic images of the far side of the Sun (Fig. 5 and Fig. 6), giving us a powerful tool for forecasting more than a week in advance their arrival at the east limb (Lindsey and Braun 2000). In the meantime, far side images are being made available on a routine basis on the SOHO web pages.

In a recent paper, Braun and Lindsey (2001) applied phase-sensitive helioseismic holography to MDI data to demonstrate how acoustic travel-time perturbations can be mapped over the entire portion of the Sun facing away from the Earth, including the polar regions. In addition to offering significant improvements to ongoing space weather forecasting efforts, the procedure offers the possibility of local seismic monitoring of both the temporal and spatial variations in the acoustic properties of the Sun over all of the far surface.

3.2 Ring Diagram Analysis

The second technique is known as 'ring diagram analysis', which is based on the study of three-dimensional power spectra of solar p-modes on a part of the solar surface. If one considers a section of a three dimensional spectrum at fixed temporal frequency, one finds that power is concentrated along a series of rings each of which corresponds to a particular

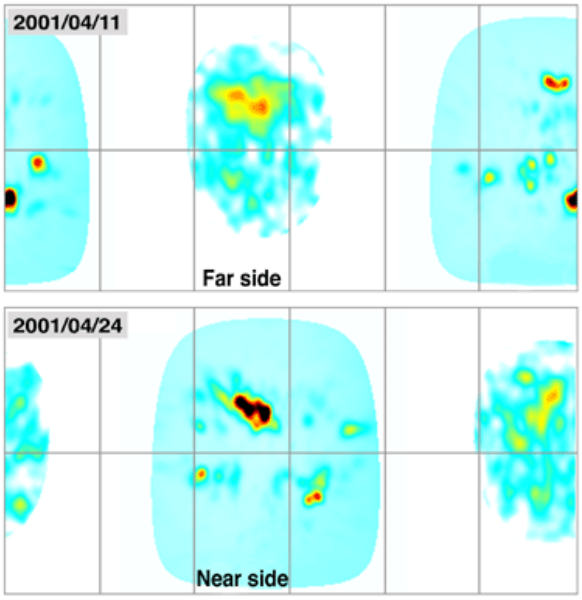

Fig. 6. The images are whole-Sun maps of magnetic activity. They show 360 degrees of longitude in the Carrington coordinate system normally used for solar observations. The farside images are maps of wave speed variations with locations showing faster wave speed shown darker. These darker regions indicate locations where there is an accumulation of magnetic field near the surface. he farside images can only be computed out to 50 degrees from the farside disk center as (un)seen from Earth.

value of the radial degree n. A horizontal velocity field (U_h) present in the region in which the modes propagate produces an advection effect of the wave front and a shift in the frequencies of the modes, $\Delta\omega = k_h \cdot U_h$. Such a displacement manifests itself as an effective displacement of the centers of the rings in the constant frequency cuts. The measured frequency shifts can be inverted to obtain the horizontal flow velocities as a function of depth. Schou and Borgart (1998), Basu et al. (1999), and Gonzales Hernandez et al. (1999) applied this technique to MDI data to determine near-surface flows in the Sun. A remarkable meridional flow from the equator to the poles was found in the outermost layers of the convection zone, reaching a maximum amplitude of 25–30 m/s at approximately 30 deg latitude. There is some dispute about whether the amplitude of the meridional flow levels off and becomes smaller at this latitude. The flows appear to diverge close to the equator (but not exactly on the equator). No change of sign of the meridional flow has been measured, i.e. no evidence of a return flow has been detected in this depth range. The rotation rate determined with the ring diagram technique agrees well with that determined from global modes, and the measurements could be extended closer to the surface, providing new insight into the shear layer immediately beneath the surface.

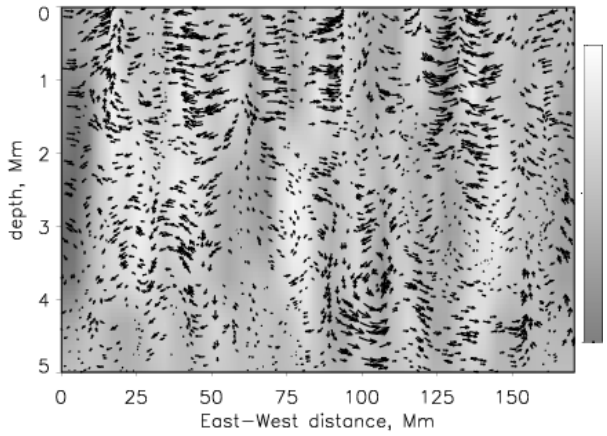

Fig. 7. A vertical cut through the upper convection zone showing subsurface flows and sound speed inhomogeneities. The flow field is shown as vectors (longest arrow 1.5 km s^{-1}) overlying the sound speed perturbations $\delta c/c$ (from Kosovichev and Duvall, 1997).

3.3 Time-distance helioseismology

The third, and perhaps most exciting and most promising technique for probing the 3-D structure and flows beneath the solar surface is called ‘time distance helioseismology’ or “solar tomography”. Basically, this new technique measures the travel time of acoustic waves between various points on the surface. In a first approximation, the waves can be considered to follow ray paths that depend only on a mean solar model, with the curvature of the ray paths being caused by the increasing sound speed with depth below the surface. The travel time is affected by various inhomogeneities along the ray path, including flow, temperature inhomogeneities, and magnetic fields. By measuring a large number of times between different locations and using an inversion method, it is possible to construct 3-dimensional maps of the subsurface inhomogeneities.

By applying this new technique to high resolution MDI data, Duvall et al. (1997) were able to generate the first maps of horizontal and vertical flow velocities as well as sound speed variations in the convection zone just below the visible surface (Fig. 7). They found that in the upper layers, 2–3 Mm deep, the horizontal flow is organized in supergranular cells, with outflows from the cell centers. The characteristic size of these cells is 20–30 Mm and the cell boundaries were found to coincide with the areas of enhanced magnetic field. The supergranulation outflow pattern disappears at a depth of approximately 5 Mm, suggesting that the depth of the supergranular layer is about 8 Mm, i.e. only about one third of the characteristic horizontal size of the cells (20–30 Mm).

One of the most successful applications of time-distance helioseismology has been the detection of large-scale meridional flows in the solar convection zone (Giles et al., 1997). Meridional flows from the equator to the poles have been observed before on the solar surface in direct Doppler shift measurements. The time-distance measurements by the

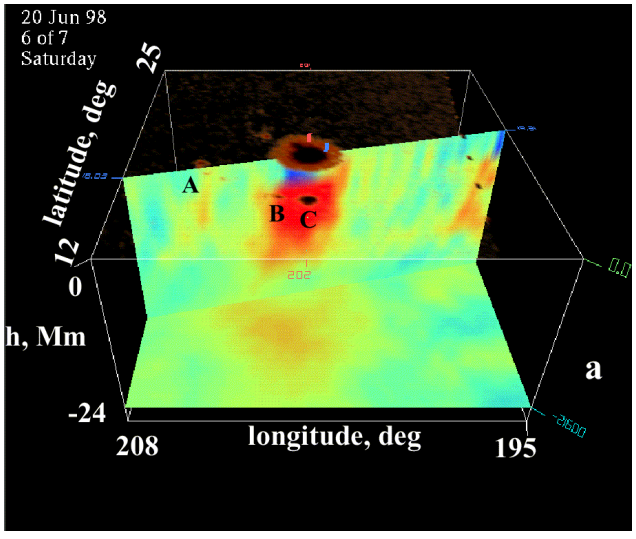

Fig. 8. Subsurface sound speed perturbations in a sunspot region observed on 20 June 1998 by MDI. The horizontal size of the box is 13 deg (158 Mm), the depth is 24 Mm. The horizontal cut is located at a depth 21.6 Mm (From Kosovichev et al. 2000).

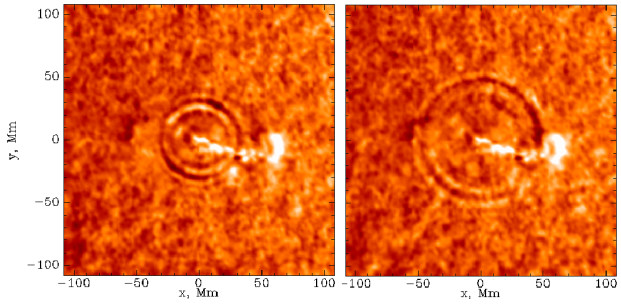

Fig. 9. Seismic waves ('sun quake') produced by a solar flare on 9 July 1996. It immediately followed a solar flare and spread out more than 120,000 km at the solar surface (Kosovichev and Zharkova, 1998).

Stanford team provided the first evidence that such flows persist to great depths, and therefore may play an important role in the 11-year solar cycle. In their initial paper they found the meridional flow to persist to a depth of at least 26 Mm, with a depth averaged velocity of 23.5 $/pm$ 0.6 m/s at mid-latitude. In the meantime these measurements have been extended down to a depth of 0.8 $R_\odot$, without finding any evidence of a return flow. Continuity considerations led them to an estimate for the return flow below 0.8 $R_\odot$ of approximately 5 m/s, which might actually be detectable in the future. Perhaps we are not too far from providing a useful constraint for dynamo theories.

One of the most exciting applications of solar tomography is its potential for studying the birth and evolution of active regions and complexes of solar activity. Kosovichev et al. (2000) studied the emergence of an active region on the disk with this technique (Fig. 8). The results show a complicated structure of the emerging region in the interior, and suggest that the emerging flux ropes travel very quickly through the upper 18 Mm of the convection zone. They estimate the speed of emergence to about 1.3 km/s, which is somewhat higher than the speed predicted by theories of emerging flux. The typical amplitude of the wave speed variations in the emerging active region is about 0.5 km s^{-1}. The observed development of the active region suggests that the sunspots are formed as a result of the concentration of magnetic flux close to the surface. The Stanford team also presented time-distance results on the subsurface structure of a large sunspot observed on 17 June 1998. The wave speed perturbations in the spot are much stronger than in the emerging flux (0.3–1 km/s). At a depth of 4 Mm, a 1 km/s wave speed perturbation corresponds to a 10% temperature variation (approx. 2800 K) or to a 18 kG magnetic field. It is interesting to note that beneath the spot the perturbation is negative in the subsurface layers and becomes positive further down in the interior. Their tomographic images also revealed sunspot 'fingers' - long, narrow structures at a depth of about 4 Mm, which connect the sunspot with surrounding pores of the same polarity. Pores which have the opposite polarity are not connected to the spot (Fig. 8).

Powerful converging and downward directed flows have been detected at depths of 1.5–5 Mm, which may provide observational evidence for the downdrafts and vortex flows that were suggested by Parker for a cluster model of sunspots (Zhao et al 2001). Strong outflows extending more than 30 Mm are found below the downward and converging flows. It is suggested that the sunspot might be a relatively shallow phenomenon, with a depth of 5–6 Mm, as defined by its thermal and hydrodynamic properties. A strong mass flow across the sunspot is found at depths of 9–12 Mm, which may provide more evidence in support of the cluster model, as opposed to the monolithic sunspot model.

MDI has also made the first observations of seismic waves from a solar flare (Kosovichev and Zharkova, 1998), opening up possibilities of studying both flares and the solar interior. During the impulsive phase of the X2.6 class flare of 9 July 1996 a high-energy electron beam heated the chromosphere, resulting in explosive evaporation of chromospheric plasma at supersonic velocities. The upward motion was balanced by a downward recoil in the lower chromosphere which excited propagating waves in the solar interior. On the surface the outgoing circular flare waves resembled ripples from a pebble thrown into a pond (Fig. 9). The seismic wave propagated to at least 120 000 km from the flare epicenter with an average speed of about 50 km/s on the solar surface.

4 Transition region

4.1 EUV spectral atlases

A far-ultraviolet and extreme-ultraviolet (FUV, EUV) spectral atlas of the Sun between 670 Å and 1609 Å in the first order of diffraction has been derived from observations ob-

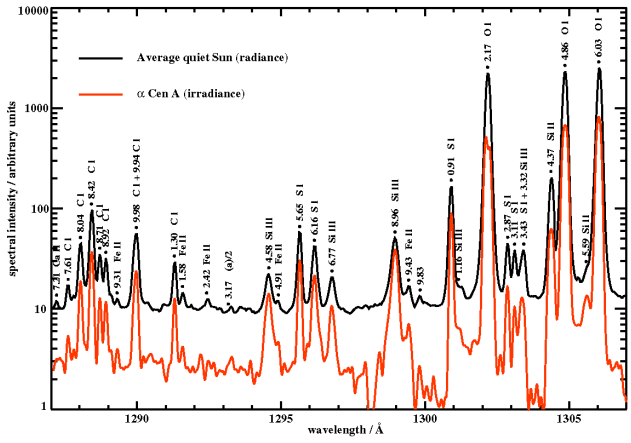

Fig. 10. A sub-section of the extensive SUMER atlas compared with the irradiance spectrum of Alpha Cen A from HST-STIS (from Curdt et al. 2001).

tained with the SUMER (Solar Ultraviolet Measurements of Emitted Radiation) spectrograph (Curdt et al. 2001). The atlas contains spectra of the average quiet Sun, a coronal hole and a sunspot on the disk. The spectra include emissions from atoms and ions in the temperature range 6×10^3 K to 2×10^6 K, i.e., continua and emission lines emitted from the lower chromosphere to the corona. This spectral atlas, with its broad wavelength coverage, provides a rich source of new diagnostic tools to study the physical parameters in the chromosphere, the transition region and the corona. In particular, the wavelength range below 1100 Å as observed by SUMER represents a significant improvement over the spectra produced in the past. A close-up of a selected region of the spectral atlas, compared with the irradiance spectrum of Alpha Cen A from HST-STIS, is shown in Fig. 10.

Brooks et al. (1999) presented a quiet Sun EUV spectrum observed by the Coronal Diagnostic Spectrometer (CDS) in the wavelength range 308-381 Å and 513–633 Å. More than 200 lines have been measured and about 50% identified. The paper includes a set of annotated spectral atlas plots with all observed lines labelled with their final corrected wavelengths and a set of tables giving line wavelengths, line count rates, line widths and background count rates together with their standard errors over position. A first observation of the intercombination line of He I at 591 Å in the solar atmosphere has been made.

4.2 The Network

Early models of the solar atmosphere assumed that the temperature structure of the upper atmosphere was continuous with a thin transition region connecting the chromosphere with the corona. It is now apparent that this depiction is too simplistic. Rather, it appears that the solar atmosphere consists of a hierarchy of isothermal, highly dynamic loop structures. Of particular interest in this context is the network, which is believed to be the backbone of the entire solar atmosphere and the basic channel of the energy responsible for heating the corona and accelerating the solar wind.

Patsourakos et al. (1999) used CDS data to study the width variation of the network with temperature. They found that the network boundaries have an almost constant width up to about 250 000 K (where the network contrast is also strongest) and then fan out rapidly at coronal temperatures. The network size in the lower transition region is about 10 arcsec and spreads to about 16 arcsec at 1 MK. These results are in very good agreement with the transition region-corona model of Gabriel (1976). The results of Feldman et al. (1999), on the other hand, are inconsistent with that model. They studied the morphology of the quiet solar atmosphere from 40 000 to 1 400 000 K and found no association with the chromospheric network above 900 000 K. The hottest loop structures seem to form a canopy over lower temperature loop structures and the cross-sectional areas of long coronal loops are constant to within the instrumental spatial resolution. Feldman et al. see difficulties reconciling these findings with the transition region-corona model of Gabriel (1976), which assumes a large scale uniform corona threaded by vertical magnetic fields. In this model, the transition region is produced by conduction back-heating from the corona. Their new observations, on the other hand, require emitting loops to be heated internally.

4.3 Doppler shifted emission in the transition region

For more than two decades it has been known that the UV emission lines originating from the transition region of the quiet Sun are systematically redshifted relative to the lower chromosphere. In earlier investigations the magnitude of the redshift has been found to increase with temperature, reaching a maximum at T $\approx 10^5$ K, and then to decrease sharply toward higher temperatures (e.g. Brekke, 1993, and references therein). Systematic redshifts have also been observed in stellar spectra of late type stars, first with the International Ultraviolet Explorer (e.g., Ayres et al., 1983, 1988; Engvold et al., 1988) and recently by the Hubble Space Telescope (Wood et al., 1996, 1997). Below temperatures of about 1.6×10^5 K, the line redshifts of the Sun, α Cen A, α Cen B, and Procyon are all very similar.

Early observations from SOHO extended the observable temperature range and suggested that the average redshift persists to higher temperatures than in most previous investigations (e.g. Brekke, Hassler, and Wilhelm, 1997; Chae et al., 1998c). Shifts in the range $+10$–16 km s^{-1} were observed in lines formed at T =1.3–2.5 $\times 10^5$ K (Fig. 11). Even upper transition region and coronal lines (O VI, Ne VIII, and Mg X) showed systematic redshifts in the quiet Sun corresponding to velocities around +5 km/s. These measurements were made using the standard reference rest wavelengths reported in the literature (e.g. Kelly, 1987).

More recent investigations using observations with SUMER have revisited this problem. There also possible errors in rest wavelengths of lines from highly ionized atoms (e.g. Ne VIII, Na IX, Mg X, Fe XII) are discussed. Peter (1999) exam-

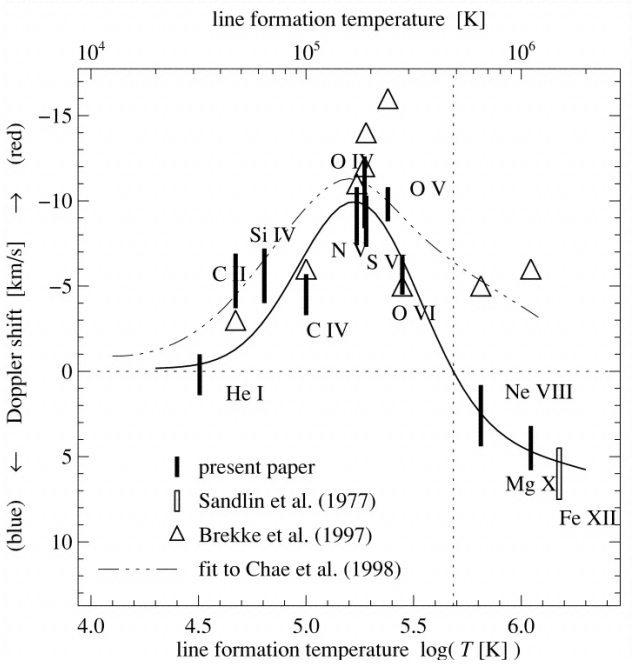

Fig. 11. Variation of the Doppler shift at disk center with formation temperature of the line. Error bars for the data of Brekke et al. (1997) were typically 2 km/s (not shown). The solid line is a by-eye fit to the Doppler shifts. (From Peter and Judge, 1999)

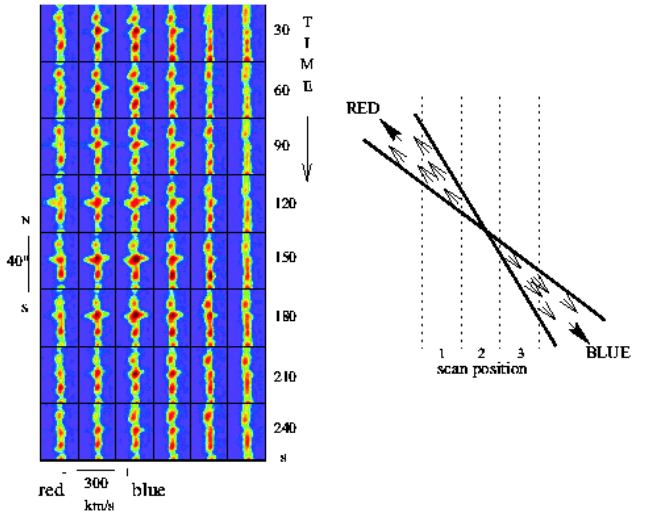

Fig. 12. Bi-directional plasma jets observed by SUMER in Si IV 1993 Å on June 1996 and a schematic of the plasma flow (Innes et al. 1997).

ined the center-to-limb variation of the Doppler shifts of C IV (1550 Å) and Ne VIII (770 Å) using full disk scans obtained with SUMER. Assuming that all effects of mass or wave motion on the limb cancel out in a statistical sense they adopt the line position on the limb as a rest wavelength. The line shifts obtained with this technique at disk center correspond to a redshift of 6 km/s for C IV and a blueshift of 2.5 km/s for Ne VIII. Similar results have been presented by Dammasch et al., (1999), Teriaca et al., (1999), and Peter and Judge (1999) who also found the Mg X line to be blueshifted by 4.5 km/s on the solar disk (Fig. 11).

These recent results suggest that the upper transition region and lower corona appear blueshifted in the quiet Sun, with a steep transition from red- to blue-shifts above 5×10^5 K. This transition from net redshifts to blueshifts is significant because it has major implications for the transition region and solar wind modeling as well as for our understanding of the structure of the solar atmosphere. The results also motivates new laboratory measurements of the wavelengths of hotter lines since the choice of rest wavelengths used to derive these results are crucial for the interpretation of the data.

4.4 Explosive events and "blinkers"

Several types of transient events have been detected in the quiet Sun. High-velocity events in the solar transition region, also called "explosive events", were first observed by Brueckner and Bartoe (1983), based on UV observations with HRTS. Explosive events in quiet regions have large velocity dispersions, about ± 100 km/s, i.e. velocities are directed both towards and away from the observer causing a strong line broadening.

Explosive events have been studied extensively by a number of authors using SUMER data (e.g. Innes et al., 1997a, 1997b; Chae et al., 1998a, 1998b; Perez et al., 1999) and some results support the magnetic reconnection origin of these features. Innes et al., (1997b) reported explosive events that show spatially separated blue shifted and red shifted jets and some that show transverse motion of blue and red shifts (Fig. 12), as predicted if reconnection was the source (Dere et al., 1991). Comparison with MDI magnetograms and magnetograms obtained at Big Bear Solar Observatory also provided evidence that transition region explosive events are a manifestation of magnetic reconnection occurring in the quiet Sun (Chae et al., 1998a). The explosive events were found to rarely occur in the interior of strong magnetic flux concentrations. They are preferentially found in regions with weak and mixed polarity, and the majority of these events occur during "cancellation" of photospheric magnetic flux (Chae et al., 1999).

Harrison et al. (1999) presented a thorough and comprehensive study of EUV flashes, also known as "blinkers", which were identified in quiet Sun network as intensity enhancements of order 10–40% using CDS. They have analyzed 97 blinker events and identified blinker spectral, temporal and spatial characteristics, their distribution, frequency and general properties, across a broad range of temperatures, from 20 000 K to 1 200 000 K. The blinkers are most pronounced in the transition region lines O III, O IV and O V, with modest or no detectable signature at higher and lower temperatures. A typical blinker has a duration of about 1000 s. Due to a long tail of longer duration events, the average duration is 2400 s, though. Comparison to plasma cooling times

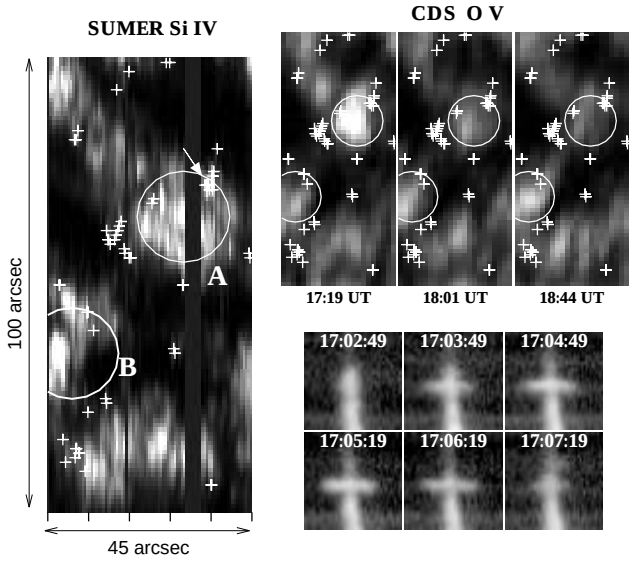

Fig. 13. Observations of "blinkers" with SUMER and CDS. The SUMER Si IV integrated line intensity image of a quiet Sun area (left panel) shows the transient network brightening (circles A and B). The symbols (+) mark the locations of the detected explosive events. The right upper panel show the corresponding areas observed with CDS where same brightenings are clearly visible. Note that the explosive events tent to avoid the centers of the network brightenings. The lower right panel shows a time sequence of the Si IV line during an explosive event (Chae et al. 1998a).

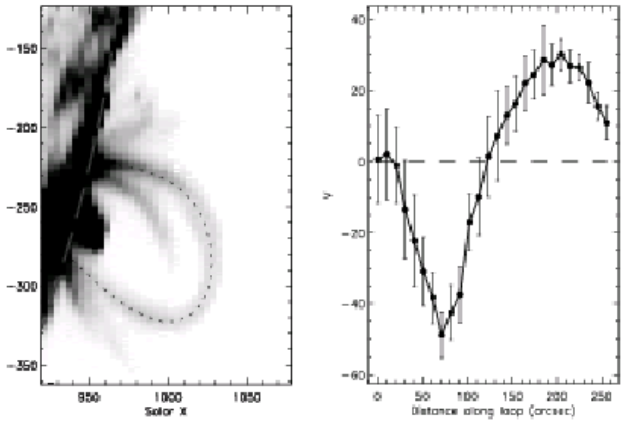

Fig. 14. Emission and variation of the line of sight velocity along a loop in the O^{+4} line at 63 nm, emitted at $T \sim 235\,000$ K.

led to the conclusion that there must be continuous energy input throughout the blinker event. The projected blinker onset rate for the entire solar surface is $1.24\,s^{-1}$, i.e. at any one time there are about 3000 blinker events in progress. Remarkably, line ratios from O III, O IV and O V show no significant change throughout the blinker event, suggesting that the intensity increase is not a temperature effect but predominantly caused by increases in density or filling factor. The authors estimate the thermal energy content of an average blinker at 2×10^{25} erg.

While the explosive events appear as extremely broad line profiles with Doppler shifts of ± 150 km/s without significant brightenings, spectral line fits to CDS data, have so far revealed no clear velocity shifts or only modest velocities up to a maximum of 20 km/s. Typically, the explosive events are short lived (≈ 60 s), small scale (about 2 arcsec) and occur at a rate of 600 s^{-1} over the Suns surface. Chae et al. (1999) compared SUMER explosive events with coordinated CDS observations and magnetograms from Big Bear. They found that the explosive events tend to avoid the centers of network brightening and are mostly located at the edges of such brightenings based on observing sequences obtained on two different days (Fig. 13). While both types of events appear to be fairly common, it seems that they are two different classes of events. Clearly, further analysis is needed to establish the relationship between these two phenomena.

4.5 Active region dynamics

Observations with CDS, SUMER, TRACE and EIT show that the solar plasma at temperatures 0.1 MK to 1.0 MK, trapped inside large magnetic loops in active regions, is extremely dynamic and time variable (e.g. Brekke, Kjeldseth-Moe, and Harrison 1997; Kjeldseth-Moe and Brekke, 1998). TRACE and EIT (at 1–1.5 MK) show emission fronts moving along the magnetic fields, while Doppler shifts of EUV lines observed with CDS and SUMER, reveal that high material velocities in fact occur. Line of sight velocities of -40 to $+40$ km/s, as in the Fig. 14, are typical. The variation of the velocity with position is, however, *not* consistent with a siphon or any extended flow along the loop.

Velocities and intensities in the loops change in 2–5 minutes, consistent with the changes observed with EIT and TRACE. Variability is persistent and may last for hours and days. Life times of individual loops at transition region temperatures range from 10 min to 3 hours. However, the loops often form and disappear quickly, in about 10 min. There is no time sequence of loops at different temperatures, i.e. no sign of a structure running through a range of temperatures with time.

Structures at different temperatures are generally co-located over a wide range of temperatures $T \leq 1$ MK. They often emit along their full length, thus appearing isothermal (see Fig. 14). Loops containing coronal temperature plasmas appear to change more slowly. However, this impression may be caused by a large number of (overlapping) loops with changes only in those loops that are magnetically connected to the active transition region loops.

The observations point towards a conceptual picture of loops as collections of thin, thermally insulated strands that extend over long sections owing to high thermal conductivity. Heating episodes cause the strands to have different specific temperatures and excite flows and waves causing the observed Doppler shifts.

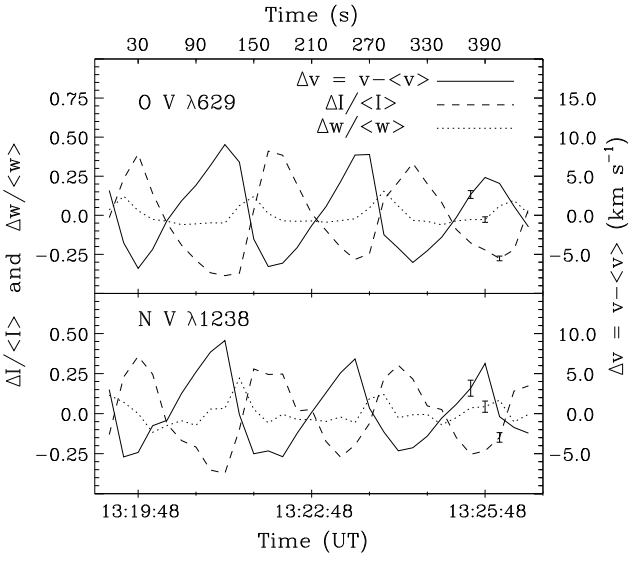

Fig. 15. Observed oscillations in relative line-of-sight velocity $\Delta\nu = \nu - \langle v \rangle$ (solid line), relative peak intensity $\Delta I/\langle I \rangle$ (dashed line), and relative line width $\Delta w/\langle w \rangle$ (dotted line), in the center of a sunspot umbra.(From Brynildsen et al., 1999)

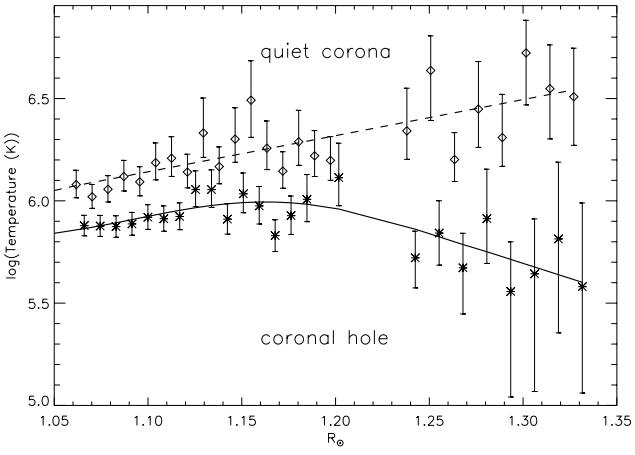

Fig. 16. Temperature gradient measurement in the quiet corona (equatorial west limb) and the north polar coronal hole. (From David et al., 1998)

Brynildsen, Kjeldseth-Moe, and Maltby (1999) studied 3-min transition region oscillations above sunspots by analyzing time series recorded in O v 629 Å, N v 1238 Åand 1242 Å, and the chromospheric Si II 1260 Åline in NOAA 8378. The 3-min oscillations they observed above the sunspot umbra show (a) larger peak line intensity amplitudes than reported before, (b) clear signs of nonlinearities, (c) significant oscillations in line width, and (d) maxima in peak line intensity and maxima in velocity directed toward the observer that are nearly in phase (Fig. 15). They also performed a simple test and calculated the velocity oscillations from the intensity oscillations (which, to a first approximation for optically thin lines, was proportional to ρ^2) using a standard text book equation for simple nonlinear acoustic waves. The agreement to the observed velocity is astounding, providing convincing evidence that the oscillations they observed are upward-propagating, nonlinear acoustic waves.

Extensive observing programmes of the 3-minute oscillations in the chromosphere and transition region by Maltby et al. (1999), Brynildsen et al. (2000) and Fludra (2001) have given new information about the oscillations above sunspots. The results are compatible with linear acoustic waves in most sunspots, a few sunspots show nonlinear waves. Maltby et al. (2001) found that the sunspot transition region oscillations end at the umbral rim and that sunspot plumes located above the umbra show the oscillations, whereas sunspot plumes located above the penumbra did not show any oscillations.

5 Corona

5.1 The helium abundance in the corona

Laming and Feldman (2001) used SUMER to obtain two independent values for the He/H abundance ratio in the corona. From comparison of He and O lines, and an adjustment of the electron collision rates for He II (to include more levels, cascades, and radiative recombination), they obtain a ratio [He/H] = 0.038 ± 0.006. From comparison of line strengths of He and the H I Balmer series, they arrive at a value of 0.052 ± 0.005, similar to He abundances determined in the slow solar wind. The lower value from the first method is likely due to gravitational settling of O in the solar atmosphere.

5.2 Coronal hole temperature and density measurements

Using the two spectrometers CDS and SUMER, David et al. (1998) have measured the electron temperature as a function of height above the limb in a polar coronal hole (Fig. 16). Temperatures of around 0.8 MK were found close to the limb, rising to a maximum of less than 1 MK at 1.15 $R_\odot$, then falling to around 0.4 MK at 1.3 $R_\odot$. In equatorial streamers, on the other hand, the temperature was found to rise constantly with increasing distance, from about 1 MK close to the limb to over 3 MK at 1.3 $R_\odot$. With these low temperatures, the classical Parker mechanims cannot alone explain the high wind velocities, which must therefore be due to the direct transfer of momentum from MHD waves to the ambient plasma.

Marsch et al., (1999) analyzed SUMER measurements of the Lyman series (H I Ly6, Ly7, and Ly9) obtained near the limb from about 10 to 70 arcsec and compared them to multilevel NLTE radiative transfer calculations, allowing them to derive consistently the temperatures and densitites of the hydrogen atoms at the base of the corona. The Lyman lines are broad and show the typical self-absorption reversal near

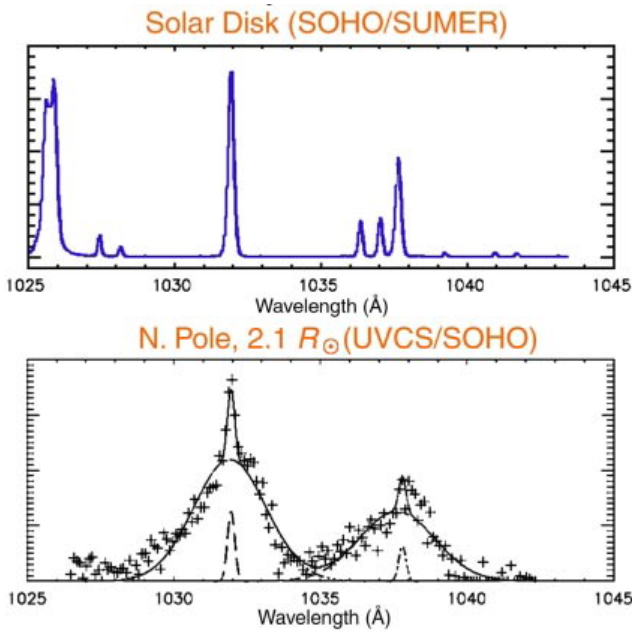

Fig. 17. Line profiles of O VI 1032 Å and 1037 Å above the north polar coronal hole at 2.1 $R_\odot$ observed by UVCS (lower panel). Upper panel shows tha same emission lines observed on the disc by SUMER. The broad O VI line widths observed by UVCS indicate velocities of up to 500 km/s, equivalent to a thermal-motion kinetic temperature of 200 million K. The narrow peaks in the lower panel are due to stray light (Kohl et al., 1997).

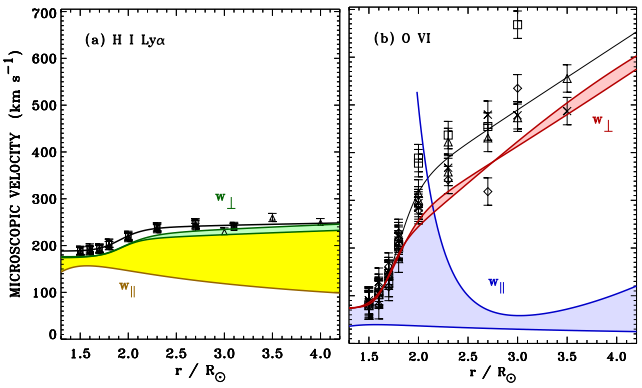

Fig. 18. $v_{1/e}$ and most probable speeds for H I Lyα (left) and O VI 1032 Å (right). Squares: north polar holes, triangles: south polar holes. Solid line: best fit to data. Dotted line: most probable speed w_e corresponding to the electron temperature. (From Kohl et al., 1998)

the limb, where the emission comes from optically thick material, and change systematically with increasing height. The Ly6, 7, and 9 line profiles become Gaussian at about 19 to 22 arcsec above the limb. The measured temperature values range between 1×10^5 and 2×10^5 K, the densities from the model calculations were found in the range 1–2 $\times 10^8$ cm^{-3}. The turbulent contribution, ξ, to the line broadenings was found to range between 20 km/s and 40 km/s, i.e. amplitues that are consistent with other estimates (Seely et al., 1997; Tu et al., 1998; Wilhelm et al., 1998a; Teriaca et al., 1999) obtained in the lower coronal holes from heavy ion EUV lines formed around 10^5 K and sufficient, according to models of e.g. Tu and Marsch (1997) and Marsch and Tu (1997) to accelerate the wind to high terminal speeds between 600 and 800 km/s.

One of the most surprising results from SOHO has been the extremely broad coronal profiles of highliy ionized elements such as oxygen and magnesium (Fig. 17). Kohl et al. (1998, 1999) and Cranmer et al. (1999a) presented a self-consistent empirical model of a polar coronal hole near solar minimum, based on H I and O VI UVCS spectroscopic observations. Their model describes the radial and latitudinal distribution of the density of electrons, H I and O VI as well as the outflow velocity and unresolved anisotropic most probable velocities for H I and O VI (Fig. 18). It provides strong evidence of anisotropic velocity distributions for protons and O VI in polar coronal holes and indicates proton outflow speeds of 190 $\pm$ 50 km/s and larger outflow speeds of 50 $\pm$ 100 km/s for O VI at 2.5 $R_\odot$ (cf. Section 6.1). While the protons (which are closely coupled to H I atoms by charge transfer in the inner corona) are only mildly anisotropic above 2–3 $R_\odot$ and never exceed 3 MK, the O VI ions are strongly anisotropic at these heights, with perpendicular kinetic temperatures approaching 200 MK at 3 $R_\odot$ and $(T_\perp/T_\parallel)$ approx. 10–100. The measured O VI and Mg X 'temperatures' are neither mass proportional nor mass-to-charge proportional when compared to H I. This and the highly anisotropic velocity distributions rule out thermal (common temperature) Doppler motions and bulk transverse wave motions along the line of sight as dominant line-broadening mechanisms. Clearly, additional energy deposition is required which preferentially broadens the perpendicular velocity of the heavier ions (cf. Sect. 5.4).

5.3 Polar plumes

Wilhelm et al. (1998a) determined the electron temperatures, densities and ion velocities in plumes and interplume regions of polar coronal holes from SUMER spectroscopic observations of the Mg IX 706/750 Å and Si VIII 1440/1445 Å line pairs. They find the electron temperature T_e to be less than 800 000 K in a plume in the range from r = 1.03 to 1.60 $R_\odot$, decreasing with height to about 330 000 K. In the interplume lanes, the electron temperature is also low, but stays between 750 000 and 880 000 K in the same height interval. Doppler widths of O VI lines are narrower in the plumes ($v_{1/e} \approx 43$ km s^{-1}) than in the interplumes ($v_{1/e} \approx 55$ km/s), confirming earlier SUMER measurements by Hassler et al. (1997). Thermal and turbulent ion speeds of Si VIII reach values up to 80 km s, corresponding to a kinetic ion temperature of 10^7 K.

These results clearly confirm that the ions in a coronal hole are extremely hot and the electrons much cooler. They also clearly demonstrate that local thermal equilibrium does not

exist in polar coronal holes and that the assumption of Collisional Ionization Equilibrium (CIE) and the common notion that $T_e \approx T_{ion}$ can no longer be made in models of coronal holes.

It seems difficult to reconcile these low electron temperatures measured in coronal holes with the freezing-in temperatures deduced from ionic charge composition data (e.g. Geiss et al., 1995). The freezing-in concept, however, assumes that the adjacent charge states are in ionization equilibrium. A critical reevaluation of this concept appears to be justified.

Previously, plumes were considered to be the source regions of the high speed solar wind. Given the narrower line widths in plumes and the absence of any significant motions in plumes, Wilhelm et al. (1998a) suggested that the source regions of the fast solar wind are the interplume lanes rather than the plumes, since conditions there are far more suitable for a strong acceleration than those prevailing in plumes.

DeForest and Gurman (1998) observed quasi-periodic compressive waves in solar polar plumes in EIT Fe IX/X 171 Åtime sequences. The perturbations amount to 10–20% of the plumes' overall intensity and propagate outward at 75–150 km/s, taking the form of wave trains with periods of 10–15 minutes and envelopes of several cycles. The authors conclude that the perturbations are compressive waves (such as sound waves or slow-mode acoustic waves) propagating along the plumes. Assuming that the waves are sonic yields a mechanical flux nearly two orders of magnitude too small to heat the coronal hole. This agrees with other models that show coronal holes being heated primarily in the hotter, interplume regions.

Using the CDS normal-incidence spectrograph, Banerjee et al. (2001) have found oscillations in polar plumes with periods of 20–50 min or longer, both off-limb and on-disk and up to 70 min further out to at least 25 arcsec off-limb. This is the first time that long period oscillations in the interplume regions close to the limb of the Sun have been detected. They interpret these oscillations as outward propagating slow magneto-acoustic waves which may contribute significantly to the heating of the lower corona by compressive dissipation and which may also provide some of the energy flux required for the acceleration of the fast solar wind.

5.4 Heating processes

A promising theoretical explanation for the high temperatures of heavy ions and their strong velocity anisotropies (cf. Sect. 5.2 and Fig. 16) is the efficient dissipation of high-frequency waves that are resonant with ion-cyclotron Larmor motions about the coronal magnetic field lines. This effect has been studied in detail by Cranmer et al. (1999b), who constructed theoretical models of the nonequilibrium plasma state of the polar solar corona using empirical ion velocity distributions derived from UVCS and SUMER. They found that the dissipation of relatively small amplitude high-frequency Alfvèn waves (10–10 000 Hz) via gyroresonance with ion cyclotron Larmor motions can explain many of the kinetic properties of the plasma, in particular the strong anisotropies, the greater than mass proportional temperatures, and the faster outflow of heavy ions in the high speed solar wind. Because different ions have different resonant frequencies, they receive different amounts of heating and acceleration as a function of radius, exactly what is required to understand the different features of the H I and O VI velocity distributions. Further, because the ion cyclotron wave dissipation is rapid, the extended heating seems to demand a constantly replenished population of waves over several solar radii. This suggests that the waves are generated gradually throughout the wind rather than propagate up from the base of the corona.

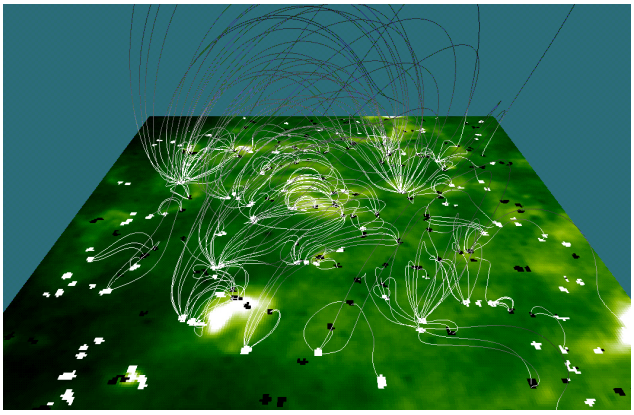

Fig. 19. Magnetic carpet. Model of magnetic field lines based on MDI magnetograms, superimposed on an image of the solar corona in Fe XII 195 Å from EIT (courtesy of SOHO/MDI consortium).

In addition to measuring velocity and intensity oscillation, MDI also measures the line-of-sight component of the photospheric magnetic field. In long, uninterrupted MDI magnetogram series a continuous flux emergence of small bipolar regions has been observed (Schrijver et al., 1998). Small magnetic bipolar flux elements are continually emerging at seemingly random locations. These elements are rapidly swept by granular and mesogranular flows to supergranular cell boundaries where they cancel and replace existing flux. The rate of flux generation of this "magnetic carpet" (Fig. 19) is such that all of the flux is replaced in about 40 hours, with profound implications for coronal heating on the top side and questions of local field generation on the lower side of the photosphere. Estimates of the energy supplied to the corona by "braiding" of large-scale coronal field through small-scale flux replacement indicate that it is much larger than that associated with granular braiding.

5.5 Coronal mass ejections

LASCO has been collecting an extensive database for establishing the best statistics ever on coronal mass ejections (CMEs) and their geomagnetic effects. St.Cyr et al. (2000) reported the properties of all the 841 CMEs observed by the LASCO C2 and C3 white-light coronagraphs from January 1996 through the SOHO mission interruption in June 1998 and compared those properties to previous observations by

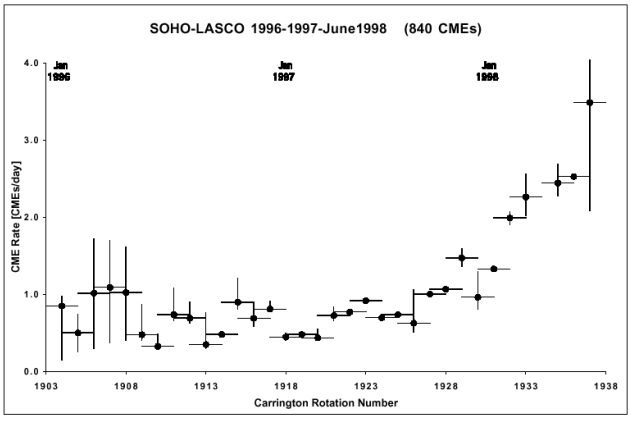

Fig. 20. CME Rate plot versus Carrington Rotation (from St.Cyr et al. 2000).

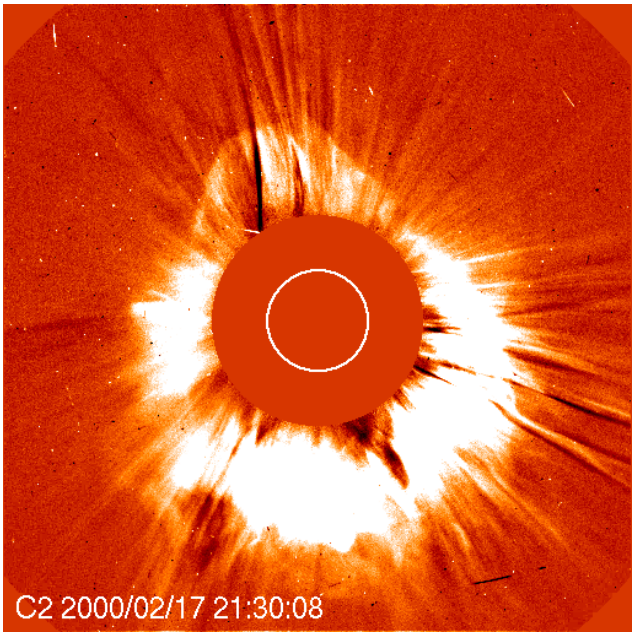

Fig. 21. Massive halo CME as recorded by LASCO C2 on 17 February 2000 (courtesy of SOHO/MDI consortium).

other instruments. The CME rate for solar minimum conditions was slightly higher than had been reported for previous solar cycles, but both the rate and the distribution of apparent locations of CMEs varied during this period as expected (Fig 20). While the pointing stability provided by the SOHO platform in its L-1 orbit and the use of CCD detectors have resulted in superior brightness sensitivity for LASCO over earlier coronagraphs, they have not detected a significant population of fainter (i.e., low mass) CMEs. The general shape of the distribution of apparent sizes for LASCO CMEs is similar to those of earlier reports, but the average (median) apparent size of 72° (50°) is significantly larger.

St.Cyr et al. also reported on a population of CMEs with large apparent sizes, which appear to have a significant longitudinal component directed along the Sun-Earth line, either toward or away from the Earth. These are the so-called 'halo CMEs' (Fig. 21). Using full disk EIT images they found that 40 out of 92 of these events might have been directed toward the Earth. A comparison of the timing of those events with the Kp geomagnetic storm index in the days following the CME yielded that 15 out of 21 (71%) of the Kp$\geq$6 storms could be accounted for as SOHO LASCO/EIT frontside halo CMEs. An additional three Kp storms may have been missed during LASCO/EIT data gaps, bringing the possible association rate to 18 out of 21 (86%).

EIT has discovered large-scale transient waves in the corona, also called 'Coronal Moreton Waves' and 'EIT waves', propagating outward from active regions below CMEs (Thompson et al., 1999). These events are usually recorded in the Fe XII 195A bandpass, during high-cadence ($\leq$20 min) observations. Their appearance is stunning in that they usually affect most of the visible solar disk (Fig. 22). They generally propagate at speeds of 200–500 km/s, traversing a solar diameter in less than an hour. Active regions distort the waves locally, bending them toward the lower Alfvén speed regions. On the basis of speed and propagation characteristics, the EIT waves were associated with fast-mode shock waves. Another interesting aspect of these coronal Moreton waves is their association with the acceleration and injection of high energy electrons and protons.

In order to investigate the interaction of the EIT waves with active regions, and the possibility of destabilization of an active region by these waves Ofman and Thompson (2001) presented the first 3D MHD modeling of this phenomena. They found that the EIT wave induces transient currents in the active region, and the resulting Lorentz force lead to the dynamic distortion of the magnetic field, and to the generation of secondary waves. The resulting magnetic compression of the plasma induces flows in the active region, which are particularly strong in the current-carrying active region.

Using LASCO data, Dere et al. (1999) found evidence for helical structures in CMEs. About one third of all CMEs seem to show this signature (St Cyr et al. 2000), which Chen et al. (2000) identify with magnetic flux ropes. This property matches that of the canonical, interplanetary magnetic cloud.

Zhang et al. (2001) studied the temporal relationship between coronal mass ejections and flares using LASCO and EIT measurements of four well-observed events. 3 of the 4 CMEs can be described in a three-phase scenario: the initiation phase, impulsive acceleration phase, and propagation phase. The initiation phase is characterized by a slow ascension with speed less than 80 km/s for a period of tens of minutes. The initiation phase always occurs before the onset of the associated flare. Following the initiation phase, the CMEs display an impulsive acceleration phase that coincides very well with the flare's rise phase lasting for a few to tens of minutes. The acceleration of CMEs ceases near the peak time of the soft X-ray flares. The CMEs then undergo a propagation phase, which is characterized by a constant speed or slowly decreasing speed. The acceleration rates

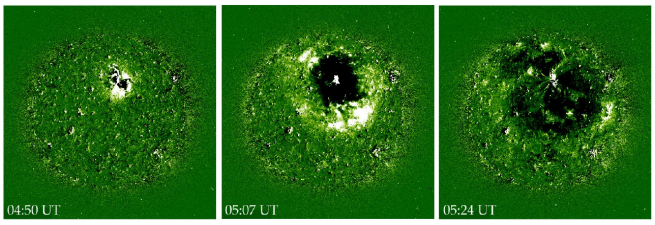

Fig. 22. Sequence of EIT difference images showing the intensity (density) enhancement and following rarefaction associated with a shock wave expanding across the solar disc from the site of the origin of a CME, recorded on 12 May 1997. The wave front travels at speeds of 300 km/s, typical of a fast Alfv/'en shock in the lower corona (Thompson et al., 1999).

in the impulsive acceleration phase are in the range 100–500 $\mathrm{m\,s^{-2}}$. The unusually strong event of 6 Nov 1997, which was associated with an X9.4 flare, did not show an initiation phase. However, it had an extremely large acceleration rate of 7300 $\mathrm{m\,s^{-2}}$.

Ciaravella et al. (2001), using UVCS, have observed an unusually narrow, bright, hot (visible in Fe XVIII, for example) feature between a CME observed in LASCO C2 and the post-CME aracade observed in EIT precisely where numerous models of rising flux ropes predict reconnection to occur.

Akmal et al. (2001) used UVCS to obtain the first observations of C III, O V, and O VI lines at 2.5 $\mathrm{R_\odot}$ above the surface in a CME. Their measurements show that the heating necessary to continue producing these lines so far from the surface is of the same order as the total kinetic energy of the CME.

6 Solar wind

6.1 Origin and speed profile of the fast wind

Coronal hole outflow velocity maps obtained with the SUMER instrument in the Ne VIII emission line at 770 Åshow a clear relationship between coronal hole outflow velocity and the chromospheric network structure, with the largest outflow velocities occuring along network boundaries and at the intersection of network boundaries (Hassler et al., 1999). This can be considered the first direct spectroscopic determination of the source regions of the fast solar wind in coronal holes.

Proton and O VI outflow velocities in coronal holes have been measured by UVCS using the Doppler dimming method (Kohl et al., 1997, 1998; Li et al., 1997; Cranmer et al.,1999a). The O VI outflow velocity was found to be significantly higher than the proton velocity, with a very steep increase between 1.5 and 2.5 $\mathrm{R_\odot}$, reaching outflow velocities of 300 km/s at around 2 $\mathrm{R_\odot}$ (Fig. 22). While the hydrogen outflow velocities are still consistent with some conventional theoretical models for polar wind acceleration, the higher oxygen flow speeds cannot be explained by these models. A possible explanation is offered by the dissipation of high-frequency Alfvèn waves via gyroresonance with

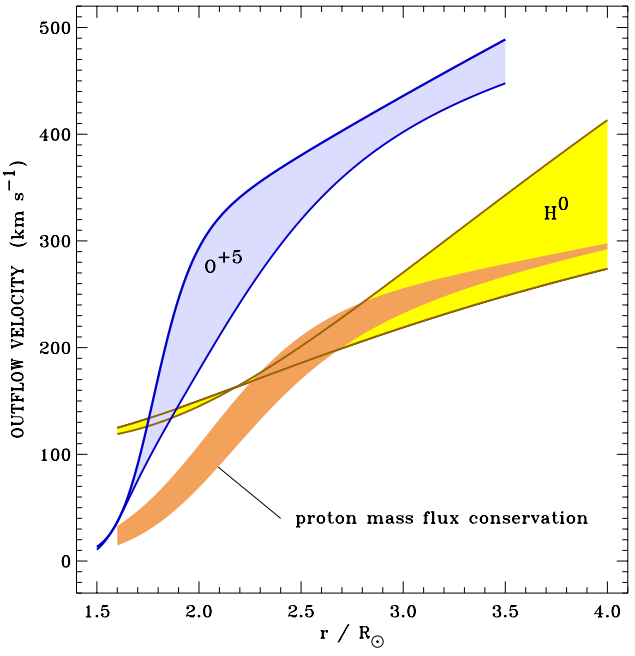

Fig. 23. Empirical outflow velocity of O VI and H I in coronal holes over the poles, with gray regions corresponding to lower/upper limits of $w_\parallel$. (From Kohl et al., 1998.)

ion cyclotron Larmor motions, which can heat and accelerate ions differently depending on their charge and mass.

Miralles et al. (2001) used UVCS to compare trans- equatorial coronal hole plasma properties to those measured in polar holes, and found that outflow speeds and perpendicular most-probable speeds in O VI were ≈3 times lower at a given height than in large polar holes at solar minimum. Since ACE measurements at 1 AU in the same low-latitude holes show wind speeds of 600–700 km/s, one must conclude that most of the wind acceleration in the low-latitude holes is occurring above 3 $\mathrm{R_\odot}$, while in the polar holes, it occurs below that height.

6.2 Speed profile of the slow solar wind

Time-lapse sequences of LASCO white-light coronagraph images give the impression of a continuous outflow of material in the streamer belt. Density enhancements, or 'blobs', form near the cusps of helmet streamers and appear to be carried outward by the ambient solar wind. Sheeley et al. (1997), using data from the LASCO C2 and C3 coronagraphs, have traced a large number of such 'blobs' from 2 to over 25 solar radii. Assuming that these 'blobs' are carried away by the solar wind like leaves on the river, they have measured the acceleration profile of the slow solar wind, which typically doubles from 150 km/s near 5 $\mathrm{R_\odot}$ to 300 km/s near 25 $\mathrm{R_\odot}$. They found a constant acceleration of about 4 $\mathrm{ms^{-2}}$ through most of the 30 $\mathrm{R_\odot}$ field-of-view. The speed profile is consistent with an isothermal solar wind expansion at a temperature of about 1.1 MK and a sonic point near 5 $\mathrm{R_\odot}$.

6.3 Inward-moving coronal features

Small-scale structures that move inward through the corona at heliocentric distances of 2–4 $R_\odot$ has been reported by Wang et al. (1999). The downflows are typically observed 12-36 hours after the onset of a CME. Most of the inward-moving features have a cusp-like appearance with an angular width of only a few degrees. Larger curved loops are also sometimes seen. The inflow speeds range from less than 20 km/s to more than 100 km/s. Most show deceleration or nearly uniform inward motion, but there also some which show acceleration.

Sheeley, Knudson, and Wang (2001) studied the occurrence rate of these inward-moving coronal features with solar activity indicators. Their study revealed that the inflowing features are especially common when the magnetic field has a four-sector structure. The measured inflow rate is correlated with the occurrence of nonpolar coronal holes and other indicators of the Sun's nonaxisymmetric open flux, but less so with conventional indicators of solar activity like the sunspot number of coronal mass ejection rate. They conclude that most inflows indicate collapsing field lines that occur as nonpolar coronal holes are subjected to photospheric motions and the eruptions of new flux.

6.4 Solar wind composition

Kallenbach et al. (1997), using CELIAS/MTOF data, has made the first in-situ determination of the solar wind calcium isotopic composition, which is important for studies of stellar modelling and solar system formation, because the present-day solar Ca isotopic abundances are unchanged from their original isotopic composition in the solar nebula. The isotopic ratios ^{40}Ca/^{42}Ca and ^{40}Ca/^{44}Ca measured in the solar wind are consistent with terrestrial values.

The first in-situ determination of the isotopic composition of nitrogen in the solar wind has been made by Kallenbach et al., (1998), also based on CELIAS/MTOF data. They found an isotope ratio $^{14}\mathrm{N}/^{15}\mathrm{N} = 200 \pm 60$, indicating a depletion of ^{15}N in the terrestrial atmosphere compared to solar matter.

Aellig et al., (1998) have measured iron freeze-in temperature with CELIAS/CTOF with a time resolution of 5 min. Their measurements indicate that some of the filamentary structures of the inner corona observed in Hα survive in the interplanetary medium as far as 1 AU.

Aellig et al., (1999) derived from CELIAS/CTOF data a value for the elemental Fe/O ratio in the solar wind. Since Fe is a low FIP element and O a high FIP element their relative abundance is diagnostic for the FIP fractionation process. The unprecedented time resolution of the CELIAS data allowed a fine scaled study of the Fe/O ratio as a function of the solar wind bulk speed. The Fe/O abundance shows a continuos decrease with increasing solar wind speed by a factor of two between 350 km/s and 500 km/s, in correspondence to the well-known FIP effect.

Using solar wind particle data from CELIAS/MTOF, Wurz et al., (1998) determined the abundance of the elements O, Ne, Mg, Si, S, Ca, and Fe of the January 6, 1997, CME. During the passage of the CME and the associated erupted filament, they measured an elemental composition which differs significantly from the interstream and coronal hole regions before and after this event. During the event they found a mass-dependent element fractionation with a monotonic increase toward heavier elements. The observed Si/O and Fe/O abundance ratios were about 0.4 during the CME and 0.5 during the filament passage, which is significantly higher than for typical solar wind streams.

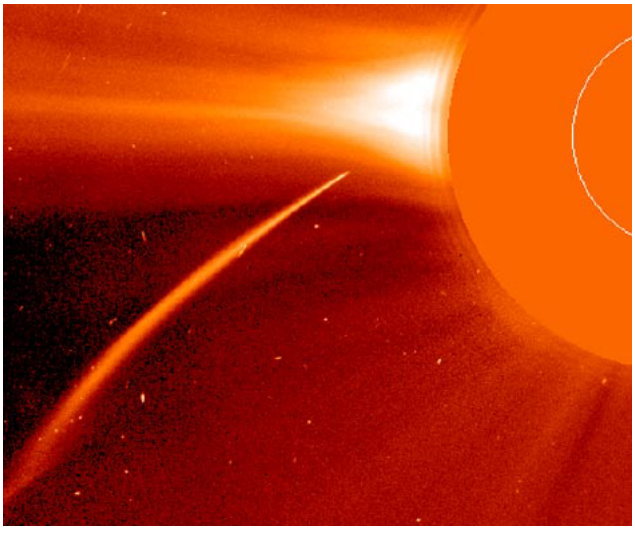

Fig. 24. Comet SOHO-6, one of numerous sungrazing comets discovered by LASCO, as its head enters the equatorial solar wind region. The image was recorded on 23 December 1996 (Courtesy SOHO/LASCO consortium).

7 Comets

SOHO is providing new measurements not only about the Sun. SOHO has discovered more than 350 comets by September 2001, most of them belonging to sun-grazing comets of the Kreutz family. One particular feature of these observations is the presence of a dust tail for only a few sungrazers while no tail is evident for the majority of them. Analysis of the light curves is used to investigate the properties of the nuclei (size, fragmentation, destruction) and the dust production rates.

Biesecker et al. (2001) studied sungrazing comets in LASCO images and found that the number of Kreutz family members discovered each year has remained approximately constant. None of the comets have been detected post-perihelion. The individual comets can be related to one of two "standard candles," which they call Universal Curves. The comets all reach a peak brightness at one of two characteristic distances (both near 12 solar radii). In addition, the comets fragment at another characteristic distance (about 6 solar radii), due to thermal or gravitational stress (or both).

The study also found evidence for line emission which varies with heliocentric distance.

Thanks to rapid communication from the LASCO group and the near-realtime observing capabilities of the SOHO instruments due to the unique operations concept of SOHO, UVCS could make spectroscopy measurements of several comets on the day of their discovery. UVCS spectroscopic measurements of comet C/1996Y1 obtained at $6.8\,R_\odot$ confirmed the predictions of models of the cometary bow shock driven by mass-loading as cometary molecules are ionized and swept up in the solar wind. From the width and shift of the line profiles the solar wind speed at $6.8\,R_\odot$ could be determined (640 km/s). The outgassing rate of the comet was estimated at 20 kg/s, implying an active area of the nucleus of only about 6.7 m in diameter and a mass of about 120 000 kg (Raymond et al. 1998).

Uzzo et al. (2001, ApJ 558, 403-410) report UVCS Ly-alpha observations of comet C/2000 C6, a member of the Kreutz family of sungrazing comets, which was in the UVCS FOV 9–10 Feb 2000. A tail nearly 0.5 R in length was detected in Ly-alpha emission. From the Ly-alpha intensity and its rate of fading due to H I ionization they estimated the streamer density at $4.56\,R_\odot$ to $0.68 \times 10^5\,cm^{-3}$. They also determined the outgassing rate at various heights, which in turn gives and estimate of the diameter of the nucleus (12 m). Further, between 5.7 and $4.6\,R_\odot$ a sudden brightening was observed, which is interpreted as fragmentation of the nucleus.

Comets are surrounded by large clouds of hydrogen, produced by the break-up of water molecules evaporating from the comets' ice. The solar wind mapper SWAN sees these large clouds of hydrogen glowing in the light of the H I Lyman-α line. Although generated by a comet nucleus perhaps only 40 kilometres in diameter, the hydrogen cloud of comet Hale-Bopp was 70 times wider than the Sun itself and ten times wider than the hydrogen cloud of Comet Hyakutake observed by SWAN on SOHO in 1996. The water evapouration rate of Hale-Bopp was measured by SWAN to 200 tons per day. Comet Wirtanen, the target for ESA's Rosetta mission (2003), pumped out water vapour at a rate of 20 000 tons a day during its most recent periodic visit to the Sun, according to the SWAN data (Bertaux et al 2001).

The break-up of Comet LINEAR was monitored by the SWAN instrument (Mäkinen et al. 2001). The total amount of water vapour observed by SWAN from 25 May to 12 August 2000 is estimated at 3.3 million tonnes. Only about 1% of this was left on 6 August, when observations by the Hubble Space Telescope of the dying comet's fragments gave an estimate of the total volume of the fragments. Combining the two numbers give a remarkably low value for the density - about $15\,kg\,m^{-3}$, compared with $917\,kg\,m^{-3}$ for familiar non-porous ice. Even allowing for an equal amount of dust grains, $30\,kg\,m^{-3}$ is far less than the $500\,kg\,m^{-3}$ often assumed by comet scientists. For this reason, the estimated water ice content is expected to raise some controversy. Assuming a homogenous composition of the whole comet, the nucleus had a diameter of about 750 metres at the beginning of SWAN's observation series.

8 Heliosphere

The Sun is moving through the Local Interstellar Cloud (LIC) at a velocity of about $26\,km\,s^{-1}$. The solar wind builds a cavity, the heliosphere, within the ionized gas component of the LIC (e.g. von Steiger et al., 1996). The neutral atoms (e.g. He) of the LIC, on the other hand, enter the heliosphere unaffected. The He flow properties are now well constrained from a series of measurements ($v_{He} = 25.5 \pm 0.5$ km/s, $T_{He} = 6000 \pm 1000$ K; e.g. Möbius, 1996). These values are in agreement with measurements of the velocity and temperature of the LIC deduced from stellar spectroscopy (HST, e.g. Linsky et al., 1995). Hydrogen, on the other hand, is expected to be affected by coupling with the decelerated plasma via charge-exchange. Neutral hydrogen heating and deceleration therefore provides a measurement of this coupling and in turn of the plasma density in the LIC which is responsible for most of the confinement of the heliosphere.

Costa et al., (1999) analysed SWAN H-cell data and compared them with a simple hot model of the interstellar H flow in the inner heliosphere. They found hydrogen temperatures T_0 of $11,500 \pm 1500$ K, i.e. significantly above the temperature of the interstellar He flow (6000 ± 1000 K), requiring a strong heating of more than 3500 K at the heliosphere interface. Part of this excess temperature probably is due to radiative transfer effects. They also measured a deceleration of the interstellar hydrogen at the heliopause of 3.5 ± 1.0 km/s.

Of particular interest for future studies might be the temperature minimum Costa et al., (1999) measured between the upwind and downwind direction. Classical models predict a monotonic increase of the line-of-sight temperature from upwind to downwind. The authors interpret this behaviour as first evidence of the existence of two distinct populations at different velocities, as predicted by some heliosphere-interstellar gas interface models. If confirmed, this should provide a good diagnostic of the interface.

Quémerais et al., (1999), in an independent study using data from the SWAN hydrogen absorption cell, determined the apparent interstellar hydrogen velocity in the up- and downwind direction to -25.4 ± 1 km/s and +21.6$\pm$1.3 km/s, respectively. They also presented the most precise determination (since model independent) of the H flow direction. Their new estimate of the upwind direction is $252.3° \pm 0.73°$ and $8.7° \pm 0.90°$ in ecliptic coordinates, which is off by about 3°–4° from the He flow direction. The authors speculate that this might be a sign of an asymmetry of the heliospheric interface due to the ambient interstellar magnetic field.

Comparing the above hydrogen temperature and velocity measurements by SWAN with heliospheric models leads to an estimate of the interstellar plasma density of $n_e \approx 0.04\,cm^{-3}$ (Lallement, 1999). It is interesting to note that the plasma frequency for $n_e = 0.04\,cm^{-3}$ is 1.8 kHz, i.e.

exactly the value of the remarkably stable cut-off frequency observed by Voyager (cf. e.g. Gurnett et al., 1993).

9 Solar irradiance measurements

Due to its influence on the terrestrial atmosphere the solar variability may constitute important sources of climate changes. Variations in the total solar irradiance will directly influence the amount of energy absorbed by land and oceans. Furthermore the EUV spectrum at wavelengths below 1200 Å is the dominant source of energy for heating and ionization in the terrestrial upper atmosphere at altitudes above 90 km. Any changes in the amount of EUV radiation will therefore change the chemestry, dynamics and temperature of the Earth's atmosphere. A good knowledge of the solar spectral irradiance is thus of critical importance for understanding climate variability and to distangle natural variations from human made climate changes.

The VIRGO instrument on SOHO extends the record of total solar irradiance (TSI) measurements into cycle 23. In Fig. 25 measurements from six independent space-based radiometers since 1978 (top) have been combined to produce the composite TSI over two decades (bottom). They show that the Sun's output fluctuates during each 11-year sunspot cycle, changing by about 0.1% between maxima (1980 and 1990) and minima (1987 and 1997) of solar activity. Temporary dips of up to 0.3% and a few days duration are the result of large sunspots passing over the visible hemisphere. The larger number of sunspots near the peak in the 11-year cycle is accompanied by a general rise in magnetic activity that creates an increase in the luminous output that exceeds the cooling effects of sunspots. Offsets among the various data sets are the direct result of uncertainties in the absolute radiometer scale of the radiometers ($\pm$ 0.3%). Despite these biases, each data set clearly shows varying radiation levels that track the overall 11-year solar activity cycle (cf. Fröhlich and Lean, 1998).

The VIRGO instrument measures both total solar irradiance (TSI) and spectral irradiance, the latter in three bands (centered at 4020, 5000 and 8620 Å). The TSI measurements are made with two separate radiometers; this allows for precise correction for long-term drifts in response due to exposure to solar UV. Fligge, Solanki, and Unruh (2000) have used MDI magnetogram data, rather than chromospheric proxies, to model VIRGO spectral irradiance variations on a time scale of days and less with great success. This reinforces the view that most solar irradiance variations are associated with magnetic features.

EUV irradiance measuremnts are being made on a regular basis by the SEM and CDS instruments. The Solar Extreme-Ultra-Violet Monitor, SEM, is a highly stable photodiode spectrometer that continuously measures the full solar disk absolute photon flux at the prominent and scientifically important He II 304 Å line, as well as the absolute integral flux between 170 and 700 Å (Judge et al. 1998).

Brekke et al. (2000) used full-disk CDS spectra, calibrated by means of a rocket underflight, to produce "Sun as a star" EUV irradiance measurements in the band 307–380 Å and 515–632 Å with 0.3 to 0.6 Å resolution. These measurements, continued through the SOHO mission, represent the only total solar EUV spectral irradiance measurements available until the launch of TIMED with the SEE instrument.

SUMER full Sun observations have been used to derive solar irradiance of UV and EUV lines during solar minimum conditions in 1996 (Wilhelm et al. (1998b). Radiance values were obtained for the following lines: He I 584, O V 629, Ne VIII 770, S V 786, O IV 788, S VI 933, 944, H I Ly eps 938, C III 977, N V 1239, Si I 1257, and C IV 1548. The centre-to-limb variations of these lines have also been derived. The spatially resolved measurements allowed good estimates to be made of the active region contributions to the irradiance of the quiet Sun.

10 Conclusions

SOHO was set out to tackle three broad topics in solar and heliospheric physics: the structure and dynamics of the solar interior, the heating and dynamics of the solar corona, and the acceleration and composition of the solar wind. In all three areas, observations from SOHO have caused great strides in our understanding of the diverse physical processes at work in our Sun. This has been made possible by the comprehensive suite of state of the art instruments mounted on the superb and stable platform of the SOHO spacecraft, placed in the unique vantage point of the L1 halo orbit.

In complex areas of research such as solar physics, progress is not made by just a few people acting in a vacuum. The scientific achievements of the SOHO mission are the results of a concerted, multi-disciplinary effort by a large international community of solar scientists, involving sound investment in space hardware coupled with a vigorous and well-coordinated scientific operation and interpretation effort. The interplay between theory and observations has given many new insights and will continue to do so for many years.

With the treasure of SOHO data already in the SOHO archive (and many more data yet to come, hopefully covering a full solar cycle), we should be able to unravel even more mysteries of the closest star.

Acknowledgements. The great success of the SOHO mission is a tribute to the many people who designed and built this exquisite spacecraft and these excellent instruments, and to the many people who diligently work behind the scenes to keep it up and running. Special thanks go to Harold W. Benefield and his AlliedSignal Flight Operations Team, Helmut Schweitzer and Jean-Philippe Olive from the ESA/MMS Technical Support Team, the Science Operations Coordinators Laura Roberts, Joan Hollis and Piet Martens, the SOHO Science Data Coordinator Luis Sanchez, Craig Roberts, John Rowe and their colleagues from Flight Dynamics, the colleagues from DSN, Francis Vandenbussche and his recovery team for making a miracle come true, and, last but not least, to the original Project Scientists Vicente Domingo and Art Poland

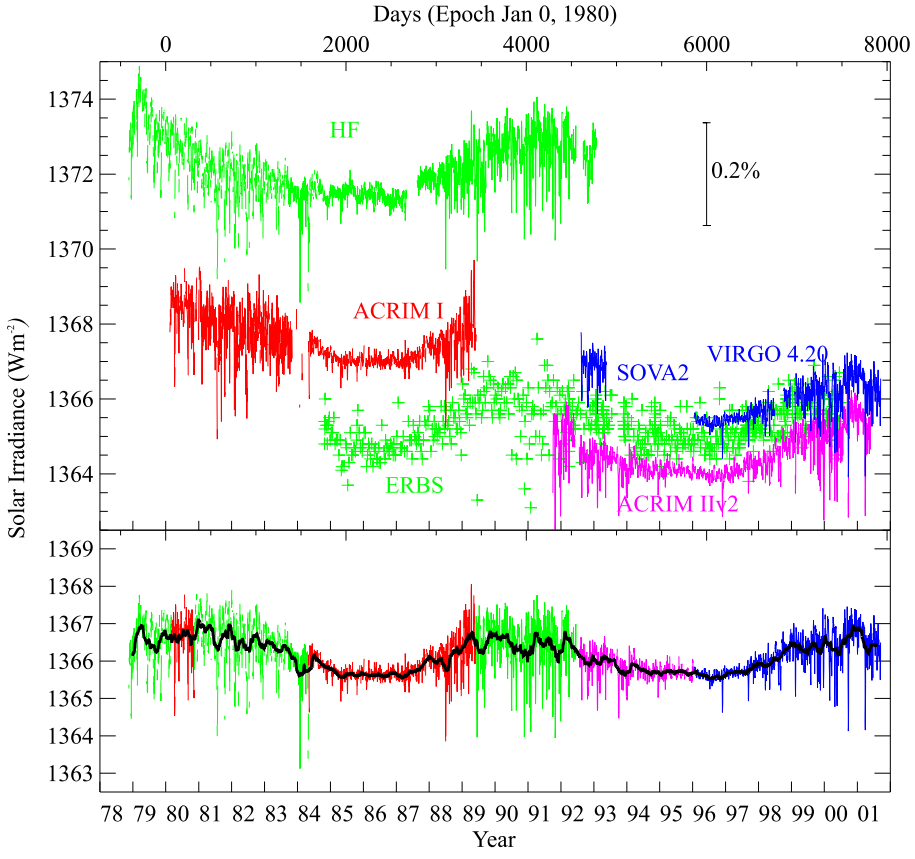

Fig. 25. Total solar irradiance variations from 1978 to 1999. The data are from the Hickey-Frieden (HF) radiometer of the Earth Radiation Budget (ERB) experiment on the Nimbus-7 spacecraft (1978-1992), the two Active Cavity Radiometer Irradiance Monitors (ACRIM I and II) placed aboard the Solar Maximum Mission satellite (SMM, 1980-1989) and the Upper Atmosphere Research Satellite (UARS, 1991-), respectively, and the VIRGO radiometers flying on the SOHO (1996-). Also shown are the data from the radiometer on the Earth Radiation Budget Satellite (ERBS, 1984-), and SOVA2 as part of the Solar Variability Experiment (SOVA) on the European Retrievable Carrier (EURECA, 1992-1993). (Updated version based on Quinn and Fröhlich, 1999)

for their leadership, which was crucial in ensuring the scientific success of this mission.

References

Aellig, M. R., Grünwald, H., Bochsler, P., et al., 1998, JGR, 103, 17 215.

Aellig, M. R., Hefti, S., Grünwald, H., et al., 1999, JGR, 104, 24 769.

Akmal, A., Raymond, J.C., Vourlidas, A., Thompson, B.J., Ciaravella, A., Ko, Y.- K., Uzzo, M., and Wu, R. 2001, ApJ, 553, 922.

Antia, H. M.; Basu, S., 2001, ApJ, 559, L67.

Ayres, T.R., Stencel, R.E., Linsky, J.L., et al., 1983, ApJ, 274, 801.

Ayres, T.R., Jensen, E., and Engvold, O., 1988, ApJ Suppl., 66, 51.

Banerjee, D., O'Shea, E., Doyle, J. G., and Goossens, M., 2001, A&A, 377, 691.

Basu, S., Antia, H.M., and Tripathy, S.C., 1999, ApJ, 512, 458.

Beck, J.G., Duvall, T.L., and Scherrer, P.H., 1998, Nature, 394, 653.

Bertello, L., Varadi, F., Ulrich, R. K., Henney, C. J., Kosovichev, A. G., Garca, R. A., Turck-Chize, S. 2000, Ap.J., 537, L143

Bertaux, J. L., Costa, J., Mäkinen, T., Quèmerais, E., Lallement, R., Kyrölä, E., and Schmidt, W., 2001, Planetary and Space Science, 47, 725.

Biesecker, D., Lamy,P., St. Cyr, O.C., Lllebaria, A., and Howard, R. 2001, Icarus, submitted

Birch, A.C. and Kosovichev, A.G., 1998, ApJ, 503, L187.

Braun, D.C., Lindesy, C., Fan, Y., and Fagan, M., 1998, ApJ, 502, 968.

Braun, D.C. and Lindsey, C., 1999, ApJ, 513, L79.

Braun, D.C. and Lindsey, C., 2001, ApJ, 560, L189.

Brekke, P., 1993, ApJ, 408, 735.

Brekke, P., Hassler, D.M., and Wilhelm, K., 1997, Solar Phys., 175, 349.

Brekke, P., Kjeldseth-Moe, O., and Harrison, R.A., 1997, Solar Phys., 175, 511.

Brekke, P., Thompson, W. T., Woods, T. N., Eparvier, F. G. 2000, ApJ., 536, 959

Brooks, D. H., Fischbacher, G. A., Fludra, A., Harrison, R. A., Innes, D. E., Landi, E., Landini, M., Lang, J., Lanzafame, A. C., Loch, S. D., McWhirter, R. W. P., Summers, H. P., and Thompson, W. T., A&A, 347, 277, 1999.

Brueckner, G.E. and Bartoe, J.-D.F., 1983, ApJ, 272, 329.

Brun, A.S., Turck-Chieze, S., and Morel, P., 1998, ApJ, 506, 913.

Brun, A.S., Turck-Chieze, S., and Zahn, J.P., 1999, ApJ, 525, 1032.

Brynildsen, N., Kjeldseth-Moe, O., and Maltby, P., 1999, ApJ, 517, L159.

Brynildsen, N., Maltby, P., Leifsen, T., Kjeldseth-Moe, O., and Wilhelm, K. 2000, Solar Phys., 191, 129.

Chae, J., Wang, H., Goode, P. R., Fludra, A. and Schuele, U., 1999, ApJ, 528, L119

Chae, J., Wang, H. , Lee, C.-Y., Goode, P.R., and Schühle, U., 1998a, ApJ, 497, L109.

Chae, J., Wang, H. , Lee, C.-Y., Goode, P.R., and Schühle, U., 1998b, ApJ, 504, L123.

Chae, J., Yun, H.S., and Poland, A.I. 1998c, ApJ Suppl., 114, 151.

Chen, J., Santoro, R. A., Krall, J., Howard, R. A., Duffin, R., Moses, J. D., Brueckner, G. E., Darnell, J. A., Burkepile, J. T. 2000, ApJ, 533, 481

Ciaravella, A. et al. 2001, Ap.J., submitted
Costa, J., Lallement, R., Quémerais, E., Bertaux, J.-L., Kyrölä, E., and Schmidt, W., 1999, A&A, 349, 660.
Covas, E., Tavakol, R., Moss, D., and Tworkowski, A., 2000, A&A, 360, L21.
Cranmer, S.R., Kohl, J.L., Noci, G., et al., 1999a, ApJ, 511, 481.
Cranmer, S.R., Field, G.B., and Kohl, J.L., 1999b, ApJ, 518, 937.
Curdt, W., Brekke, P., Feldman, U., Wilhelm, K., Dwivedi, B. N., Schühle, U., Lemaire, P., A&A, 375, 591, 2001.
Dammasch, I.E., Wilhelm, K., Curdt, W., and Hassler, D.M., 1999, A&A, 346, 285.
David, C., Gabriel, A.H., Bely-Dubau, F., Fludra, A., Lemaire, P., and Wilhelm, K., 1998, A&A, 336, L90.
DeForest, C.E. and Gurman, J.B., 1998, ApJ, 501, L217.
Dere, K.P., Bartoe, J.-D.F., Brueckner, G.E., Ewing, J., and Lund, P. 1991, JGR, 96, 9399.
Dere, K. P.,Brueckner, G. E., Howard, R. A., Michels, D. J., Delaboudiniere, J. P. 1999, ApJ, 516, 465.
Domingo,V., Fleck, B., and Poland, A.I., 1995, Solar Phys., 162, 1.
Duvall, T.L., Jr., Kosovichev, A.G., Scherrer, P.H., et al., 1997, Solar Phys., 170, 63.
Engvold, O., Ayres, T.R., Elgarøy, Ø., et al., 1988, ApJ, 192, 234.
Feldman, U., Widing, K.G., and Warren, H.P., 1999, ApJ, 522, 1133.
Fleck, B., Domingo, V., and Poland, A.I. (eds.), 1995, The SOHO Mission, Solar Phys., 162, Nos. 1–2.
Fligge, M., Solanki, S. K., Unruh, Y. C. 2000, Space Sci. Rev., 94, 129
Fludra, A. 2001, A&A, 368, 639
Fröhlich, C. and Lean, J., 1998, GRL, 25, 4377.
Gabriel, A.H., 1976, Phil. Trans. R. Soc. London A281, 575.
García, R. et al. 2001, Solar Physics, in press
Geiss, J., Gloeckler, G., von Steiger, R., et al., 1995, Science, 268, 1033.
Giles, P.M., Duvall, T.L., Jr., and Scherrer, P.H., 2000, Solar Phys., submitted.
Giles, P.M., Duvall, T.L., Jr., and Scherrer, P.H., 1997, Nature, 390, 52.
Gonzalez Hernandez, I., Patron, J., Bogart, R.S., and the SOI Ring Diagram Team, 1999, ApJ, 510, L153.
Guenther, D.B., Krauss, L.M., and Demarque, P., 1998, ApJ, 498, 871.
Gurnett, D.A., Kurth, W.S., Allendorf, S.C., and Poynter, R.L., 1993, Science, 262, 199.
Hassler, D.M., Wilhelm, K., Lemaire, P., and Schühle, U. 1997, Solar Phys., 175, 375.
Hassler, D.M., Dammasch, I., Lemaire, P., Brekke, P., Curdt, W., Mason, H.E., Vial, J.-C., and Wilhelm, K., 1999, Science, 283, 810.
Harrison, R.A., Lang, J., Brooks, D.H., and Innes, D.E., 1999, A&A, 351, 1115. Howe, R., Christensen-Dalsgaard, J, Hill, F., Komm, R. W., R. M. Larsen, J. Schou, Thompson, M. J., and Toomre, J, Science, 287, 2456, 2000a.
Howe, R., Christensen-Dalsgaard, J., Hill, F., Komm, R. W., Larsen, R. M., Schou, J., Thompson, M. J., and Toomre, J., Ap.J., 533, L163, 2000b.
Innes, D.E., Brekke, P., Germerott, D., and Wilhelm, K., 1997a, Solar Phys., 175, 341.
Innes, D.E., Inhester, B., Axford, W.I., and Wilhelm, K., 1997b, Nature, 386, 811.
Judge, D.L., McMullin, D.R., Ogawa, H.S., Hovestadt, D., Klecker,B., Hilchenbach, M., Moebius, E., Canfield,L. R., Vest, R.E., Watts, R., Tarrio, C., Khne, M., and Wurz P., 1998, Solar Phys., 177, 161.
Kallenbach, R., Ipavich, F.M., Bochsler, P., et al., 1997, ApJ, 498, L75.
Kallenbach, R., Geiss, J., Ipavich, F.M., et al., 1998, ApJ, 507, L185.
Kelly, R.L., 1987, J. of Physical and Chemical Reference Data, 16, Suppl. No. 1.
Kjeldseth-Moe, O. and Brekke, P., 1998, Solar Phys., 182, 73.
Kohl, J.-L., Noci, G., and Antonucci, E., et al., 1997, Solar Phys., 175, 613.
Kohl, J.-L., Noci, G., Antonucci, E., et al., 1998, ApJ, 501, L127.
Kohl, J.-L., Esser, R., and Cranmer, S.R., et al., 1999, ApJ, 510, L59.
Kosovichev, A.G. and Schou, J.: 1997, ApJ, 482, L207.
Kosovichev, A.G., Schou, J., Scherrer, et al., 1997, Solar Phys., 170, 43.
Kosovichev, A.G. and Zharkova, V.V., 1998, Nature, 393, 317.
Kosovichev, A.G., Duvall, T.L., and Scherrer, P.H., 2000, Solar Phys., 192, 159.
Kuhn, J.R., Bush, R.I., Scheick, X., and Scherrer, P.H., 1998, Nature, 392, 155.
Lallement, R.: 1999, in S. Habbal et al. (eds.), Proc. Solar Wind 9, AIP Conf. Proc. 471, 205.
Laming, J. M., and Feldman, U. 2001, ApJ, 546, 552.
Li, X., Esser, R., Habbal, S.R., and Hu, Y.-Q., 1997, JGR, 102, 17 419.
Lindsey, C. and Braun, D.C., 1998a, ApJ, 499, L99.
Lindsey, C. and Braun, D.C., 1998b, ApJ, 509, L129.
Lindsey, C. and Braun, D.C., 1999, ApJ, 510, 494.
Lindsey, C. and Braun, D.C., 2000, Science, 287, 1799.
Linsky, J.L., Diplas, A., Wood, B.E., et al., 1995, ApJ, 451, 335.
Mäkinen, J. T. T., Bertaux, J-L., Combi, M. R., and Qumerais, E. 2001, Science, 292, 1326.
Maltby, P., Brynildsen, N., Fredvik, T., Kjeldseth-Moe, O., Wilhelm, K., 1999, Solar Phys., 190, 437
Maltby, P., Brynildsen, N., Kjeldseth-Moe, O., Wilhelm, K., 2001, A&A, 373, L1.
Marsch, E., and Tu, C.-Y., 1997, A&A, 319, L17.
Marsch, E., Tu, C.-Y., Heinzel, P., Wilhelm, K., and Curdt, W., 1999, A&A, 347, 676.
Miralles, M.P., Cranmer, S.R., Panasyuk, A.V., Romoli, M., and Kohl, J.L. 2001, ApJ, 549, L257.
Möbius, E., 1996, Space Sci. Rev., 78, 375.
Ofman, L., and Thompson, B. J. 2001, ApJ, submitted.
Patsourakos, S., Vial, J.-C., Gabriel, A.H., and Bellamine, N., 1999, ApJ, 522, 540.
Perez, M.E., Doyle, J.G., Erdelyi, R., and Sarro, L.M., 1999, A&A, 342, 279.
Peter, H., 1999, ApJ, 516, 490.
Peter, H. and Judge, P.G., 1999, ApJ, 522, 1148.
Quémerais, E., Bertaux, J.-L., Lallement, R., and Berthé, M., 1999, JGR, 104, 12 585.
Quinn, T.J. and Fröhlich, C., 1999, Nature, 401, 841.
Raymond, J.C., Fineschi, S., Smith, P.L., et al., 1998, ApJ, 508, 410.
Roddier, F., 1975, CR Acad. Sci. Paris, 281, B993.
Schou, J., 1999, ApJ, 523, L181.
Schou, J. and Bogart, R.S., 1998, ApJ, 504, L131.
Schou, J., Antia, H.M., Basu, S., et al., 1998, ApJ, 505, 390.
Schrijver, C.J., Title, A.M., Harvey, K.L., et al., 1998, Nature, 394, 152.

Seely, J.F., Feldman, U., Schühle, U., Wilhelm, K., Curdt, W., and Lemaire, P., 1997, ApJ, 484, L87.

Sheeley, N. R., Jr., Knudson, T. N., and Wang, Y.-M. 2001, ApJ, 546, L131.

Sheeley, N.R. Jr., Wang, Y.-M., Hawley, S.H., et al., 1997, ApJ, 484, 472.

St.Cyr, C., Howard, R.A., Sheeley, N.R., Jr., et al., 2000, JGR, 105, 185.

Teriaca, L., Banerjee, D., and Doyle, J.D., 1999, A&A, 349, 636.

Thompson, B.J., Gurman, J.B., Neupert, W.M., et al., 1999, ApJ, 517, L151.

Toutain, T., T. Appourchaux, C. Frhlich, A. Kosovichev, R. Nigam, and P.H. Scherrer 1998, Ap.J., 506, L147

Tu, C.-Y., Marsch, E., 1997. Solar Phys., 109, 149.

Tu, C.-Y., Marsch, E., Wilhelm, K., and Curdt, W., 1998, ApJ, 503, 475.

Turck-Chiże, S., Couvidat, S., Kosovichev, A. G., Gabriel, A., Berthomieu, G., Brun, A.S., Chistensen-Dalsgaard, J., Garcia, R., Gough, D., Provost, J., Roca- Corts, Roxburgh, I., and Ulrich, R.K., 2001, ApJ, 555, L69

Uzzo, M., Raymond, J. C., Biesecker, D., Marsden, B., Wood, C., Ko, Y.-K., and Wu, R., 2001, ApJ, 558, 403.

von Steiger, R., Lallement, R., and Lee, M. (eds): 1996, The Heliosphere in the Local Interstellar Cloud, Space Sci. Rev., 78, Nos. 1–2.

Wang, Y.-M., Sheeley, N. R., Jr., Howard, R. A., St. Cyr, O. C., and Simnett, G. M. 1999, GRL, 26, 1203.

Wilhelm, K., Lemaire, P., Dammasch, I. E., Hollandt, J., Schuehle, U., Curdt, W., Kucera, T., Hassler, D. M., and Huber, M. C. E., 1998b, A&A, 334, 685.

Wilhelm, K., Marsch, E., Dwivedi, B.N., et al., 1998a, ApJ, 500, 1023.

Wood, B.E., Harper, G.M., Linsky, J.L., and Dempsey, R.C., 1996, ApJ, 458, 761.

Wood, B.E., Linsky, J.L., and Ayres T.R., 1997, ApJ, 487, 745.

Wurz, P., Ipavich, F.M., Galvin, A.B., et al., 1998, GRL, 25, 2557.

Zhang, J., Dere, K. P., Howard, R. A., Kundu, M. R., and White, S. M. 2001, ApJ, 559, 452.

Zhao, J., Kosovichev, A. G., Duvall, T. L. Jr. ApJ, 557, 384